Exploiting Protein Fluctuations at the Active-Site Gorge of Human Cholinesterases: Further Optimization of the Design Strategy to Develop Extremely Potent Inhibitors

Stefania Butini,[†,‡] Giuseppe Campiani,*[,†,‡] Marianna Borriello,[†,§] Sandra Gemma,[†,‡] Alessandro Panico,[†,‡] Marco Persico,[†,§] Bruno Catalanotti,[†,§] Sindu Ros,[†,‡] Margherita Brindisi,[†,‡] Marianna Agnusdei,[†,‡] Isabella Fiorini,[†,‡] Vito Nacci,[†,‡] Ettore Novellino,[†,§] Tatyana Belinskaya,[||] Ashima Saxena,[||] and Caterina Fattorusso[†,§]

European Research Centre for Drug Discovery and Development (NatSynDrugs), Università di Siena, 53100 Siena, Italy, Dipartimento Farmaco Chimico Tecnologico, via Aldo Moro, Università di Siena, 53100 Siena, Italy Dipartimento di Chimica delle Sostanze Naturali e Dipartimento di Chimica Farmaceutica e Tossicologica Università di Napoli Federico II, via D. Montesano 49, 80131 Napoli, Italy, and Division of Biochemistry, Walter Reed Army Institute of Research, Silver Spring, Maryland 20910

Received October 4, 2007

Protein conformational fluctuations are critical for biological functions, although the relationship between protein motion and function has yet to be fully explored. By a thorough bioinformatics analysis of cholinesterases (ChEs), we identified specific hot spots, responsible for protein fluctuations and functions, and those active-site residues that play a role in modulating the cooperative network among the key substructures. This drew the optimization of our design strategy to discover potent and reversible inhibitors of human acetylcholinesterase and butyrylcholinesterase (*h*AChE and *h*BuChE) that selectively interact with specific protein substructures. Accordingly, two tricyclic moieties differently spaced by functionalized linkers were investigated as molecular yardsticks to probe the finest interactions with specific hot spots in the *h*ChE gorge. A number of SAR trends were identified, and the multisite inhibitors **3a** and **3d** were found to be the most potent inhibitors of *h*BuChE and *h*AChE known to date.

Introduction

Alzheimer's disease (AD) is the most common age-related chronic neurodegenerative dementia affecting more than 20 million people worldwide. About 25−50% of the population age 85 years and over has AD[1] and, as the world population ages, it has become an urgent public health problem. Many genetic and nongenetic factors have been implicated in the pathogenesis of AD, but for the nonfamilial forms, the initial cause remains elusive.[2] AD is associated with a loss of basal forebrain cholinergic neurons and their projections, particularly in brain areas such as the neocortex, hippocampus, and amygdala, with a consequent lack of the neurotransmitter acetylcholine (ACh) around brain cells showing degenerative changes. Indeed, postmortem data revealed low levels of cholinergic markers,[3] confirming the proposed cholinergic neurochemical hypothesis of AD. Acetylcholinesterase (AChE) and butyrylcholinesterase (BuChE) are the enzymes responsible for the termination of synaptic cholinergic transmission by rapid hydrolysis of ACh and, therefore, cholinesterase (ChE) inhibition represents the currently employed approach for the treatment of AD. Because of the modest, although significant, effect of ChE inhibitors (ChEIs; e.g. donepezil, rivastigmine, and galantamine) on the cognitive status of AD patients, their benefits outweigh their risks and costs. Moreover, the NMDA receptor antagonists memantine (known as Ebixa, Axura, or Namenda) has been licensed in several countries for treatment of moderate to severe AD. Although memantine can help with the symptoms, there is no evidence that it modifies the underlying pathology of the disease.

While AChE has a well established "classical" esterase activity, the physiologic role of BuChE is still unclear. However, BuChE may have a compensatory role in the hydrolysis of ACh in brains with degenerative changes, thus making it an additional target for increasing the cholinergic tone in AD patients affected by severe symptoms.[4,5] Indeed, as AD progresses, levels of AChE decrease in some brain areas, while those of BuChE increase.[6] Although this phenomenon has been recently questioned in cortical areas,[7] an increase in BuChE was found in areas of brain associated with learning, memory, behavior, and emotional responses.[7–9] This has raised the hypothesis that inhibitory action on both enzymes could lead to an improved therapeutic benefit.[10] A rapid and long-lasting inhibition of both AChE and BuChE in the spinal fluid was shown when AD patients were given rivastigmine.[11] The improved therapeutic efficacy of this compound with respect to selective AChEIs[7,8b] accounts for the value of the dual inhibitor approach to the symptomatic treatment of AD.

These two enzymes have been extensively investigated with regard to interaction with substrates and inhibitors as well as for the multiplicity of subunit variants and oligomeric forms. The $AChE_T$ variant (T: tailed) is the only type of catalytic subunit expressed in the central nervous system (CNS),[12] where it is mostly present as a tetramer anchored to neuronal membranes through a cysteine-bound polyproline peptide named PriMA.[13] On the contrary, in AD brains, there is a decrease in $AChE_T$ with a concomitant increase in AChE associated with the extracellular insoluble material, which is enzymatically different from the enzyme associated with normal neuronal cells. Indeed, the existence of multiple AChE splice variants, together with the association of AChE substructures with additional domains and proteins, results in an array of conformationally distinct oligomeric forms with different functions, including the ability to sense and to respond to various stress insults.[14,15] On the other hand, BuChE exists as a single type of catalytic subunit, corresponding to the $AChE_T$ variant, and can be found

* To whom correspondence should be addressed. Phone: 0039-0577-234172. Fax: 0039-0577-234333. E-mail: campiani@unisi.it.
[†] European Research Centre for Drug Discovery and Development (NatSynDrugs).
[‡] Università degli Studi di Siena.
[§] Università degli Studi di Napoli "Federico II".
[||] Walter Reed Army Institute of Research.

10.1021/jm701253t CCC: $40.75
Published on Web 05/15/2008

Chart 1. Title and Reference Compounds

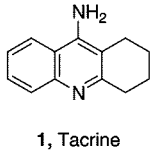

1, Tacrine

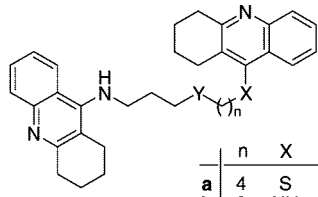

2, Reference compounds

	n	X	Y
a	4	S	CH_2
b	3	NH	NMe
c	3	S	NCOMe
d	4	S	NMe
e	4	S	NCOMe

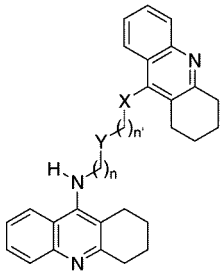

3, Title compounds

	n	n'	X	Y
a	4	3	S	NCOMe
b	4	3	S	NH
c	4	3	NH	NCOMe
d	4	3	NH	NMe
e	4	3	NH	NEt
f	4	3	NH	N-allyl
g	4	3	NH	N-β-hydroxyethyl
h	3	3	NH	1,4-piperazine
i	2	2	NH	1,3-benzene
j	2	2	NH	2,6-pyridine
k	2	2	NH	1,4-benzene
l	2	2	NH	5-Me-1,3-benzene
m	2	2	NH	3,4-furan

in a similar multitude of molecular forms.[16,17] It was recently demonstrated that, like AChE, BuChE also forms amphiphilic tetramers in the CNS bound to PriMA peptide.[13] Accordingly, AChE and BuChE must be considered multifunctional enzymes characterized by their classical esterase activity for terminating synaptic transmission and by nonclassical functions that are unrelated to their hydrolytic function.[17] In normal and pathological conditions, the nonclassical roles of AChE include modulation of glial activation, participation in hematopoiesis, neuritic outgrowth, tau phosphorylation, adhesion protein-like activity, and promotion of amyloid-β aggregation. All these actions involve the peripheral anionic site (PAS) or other AChE surface sites[18] and are related to specific protein conformations, sensitive to the concentration of metal ions.[19–24] Consequently, ChEIs may possibly have a variety of effects in the CNS.

The array of protein conformations present in different structural/functional forms of these enzymes suggests the existence of a high degree of flexibility in ChE structure and, coherently, multiple AChE motions have been demonstrated.[25] The relationship between AChE fluctuations, especially in the gorge and its functions, has been the subject of intense research by biochemists (Radic and co-workers),[26] by structural chemists (Sussman and Silman),[17,27] and by computational chemists (McCammon and co-workers).[28] The binding of a ligand to a specific site induces substantial conformational changes in other AChE substructures (e.g., mutual allosteric modulation between the catalytic site (CAS) and the PAS through the mid gorge amino acid residues). In particular, the "cross-talk" between W286 at the PAS and W86 at the CAS (human AChE numbering) has been shown to play a crucial role in the allosteric modulation of AChE activity.[26] Indeed, PAS ligands allosterically interfere with the transition between active and nonactive conformations of key residues at the CAS such as W86 and Y337.[29–31] Similarly, conformational transitions at the PAS are coupled to the closure of the cysteine loop C69−C96 (Ω-loop) over W286.[32,33] Accordingly, macroscopic protein motions were demonstrated in the gorge of mouse AChE (*m*AChE) when fasciculin-II or propidium was bound to the PAS.[34,26b] Interestingly, the existence of a residual catalytic activity of the enzyme in complex with the large fasciculin molecule may also argue for the accessibility to the CAS by alternative routes (e.g., back door).[25]

A promising strategy for interfering with biological processes is through the control of intra- and intermolecular protein−protein interactions by means of small molecules. Studies on protein−small molecule interactions and protein−protein substructure interactions suggest that there are energetic focal points, called "hot spots", on protein surfaces that are major contributors to the binding energy of the complex. Indeed, Wells and coworkers[35] demonstrated that only a small set of "hot spot" residues is able to significantly contribute to the binding energy.

Although many of the small molecule modulators known to date have been found by rational design approaches, from a pharmaceutical perspective, targeting protein hot spots[36] may be a superior route to the development of therapeutic agents compared with other strategies.

Our integrated approach was aimed at rationally design small molecules able to interfere with enzyme conformational fluctuations, thus modulating its functions and is based on the control of protein−protein interactions between ChE substructures (i.e., hot spots). During the recent development of potent tacrine-based heterobivalent ligands (HBLs), we identified multiple interaction sites in human (*h*) AChE and BuChE that were available for binding to inhibitors.[37] Accordingly, to design novel and extremely potent *h*ChEIs, we accounted for the conformational heterogeneity of ChEs in our computational and bioinformatics analysis and focused on the allosteric modulation of the three main domains lining the gorge. We uncovered specific hot spots responsible for protein fluctuations and functions, at the gorge level in both families of enzymes, and those active-site residues that play a role in modulating the cooperative network among the key substructures. For this purpose, we investigated the amino acid (AA) clusters directly involved in protein fluctuations that may be part of protein−protein interaction domains/motifs, thus representing enzyme hot spots. The original design hypothesis was that multiple interactions of an inhibitor with specific gorge hot spots may trap crucial enzyme residues in a minor abundant conformation, reducing the ability of the enzyme−inhibitor complex to access protein fluctuations, thus improving inhibitor potency.[38] Because the conformational heterogeneity in ChEs is directly linked to specific classical or nonclassical functions, a very potent inhibitor should in principle be able to freeze the "classical" enzyme structure in a particular conformational state, thus preventing ACh hydrolysis as well as nonclassical protein functions.[39]

Thus, the present study describes a thorough investigation of the active-site gorges of human ChEs with the identification of key hot spots, the targeting of which led to the development of some of the most potent inhibitors of these enzymes known to date. On the basis of our working hypothesis and analyzing the structural motions of the identified hot spots, we further optimized our previous design strategy to develop **3d** (Chart 1), the most potent inhibitor for *h*AChE, and its analogues, characterized by a different selectivity profile. This approach may pave the way to the design of selective inhibitors directed toward the catalytic and/or noncatalytic functions of *h*ChEs.

Chemistry

The synthesis of compounds **3a**−**m** (Chart 1) is reported in the following Schemes 1–3.

Compounds **3a**−**b** were synthesized as described in Scheme 1. For the synthesis of intermediate **5**,[40] we developed a new

Scheme 1. Synthesis of Heterodimers **3a**,**b**[a]

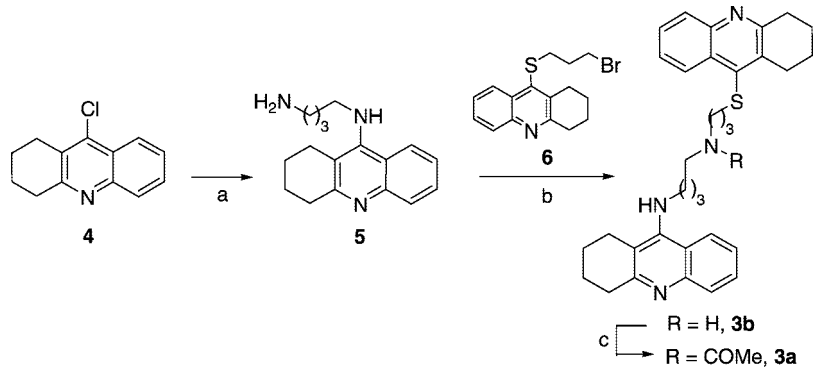

[a] (a) $Pd(OAc)_2$, (±)-BINAP, K_2CO_3, 1,4-diaminobutane, dioxane, reflux, 12 h; (b) MeCN, K_2CO_3, 18-crown-6 ether, reflux, 3 h; (c) MeCOCl, Et_3N, CH_2Cl_2, rt, 12 h.

Scheme 2. Synthesis of Compounds **3c**−**g**[a]

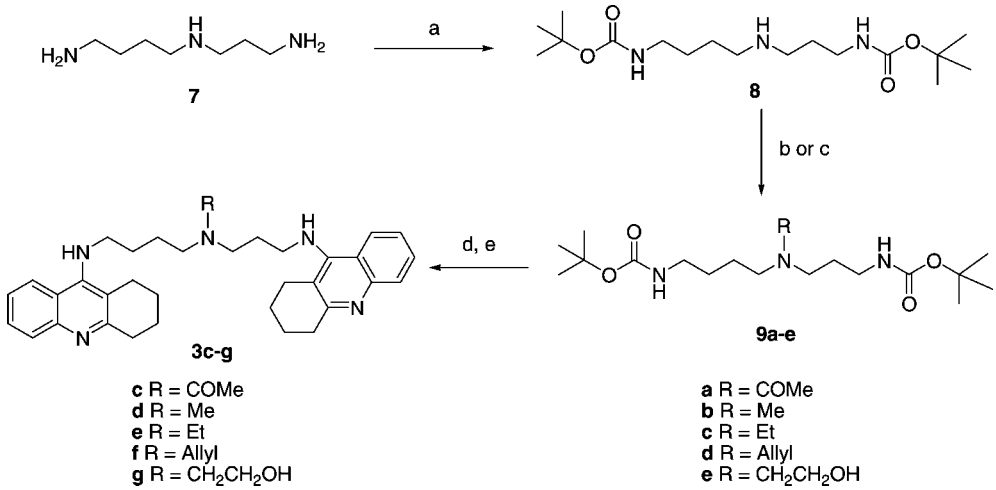

[a] (a) *t*-BuOH, CDI, KOH, toluene, 60 °C, 3 h; (b) MeCOCl, Et_3N, CH_2Cl_2, rt, 18 h for **9a**; (c) RX, K_2CO_3, MeCN, rt, 18 h for **9b**−**e**; (d) CF_3COOH, CH_2Cl_2, rt, 1 h; (e) **4**, Et_3N, pentanol, 160 °C, 18−32 h.

synthetic protocol based on a palladium-catalyzed reaction.[41] Accordingly, starting from 9-chloro-1,2,3,4-tetrahydroacridine (**4**), which was synthesized from the commercially available 1,2,3,4-tetrahydroacridanone,[42] and 1,4-diaminobutane (slight molar excess), we obtained amine **5**, which was then alkylated, to yield **3b**, using bromo-derivative **6**, obtained as previously described.[37a] Analogue **3a** was obtained starting from **3b**, using an acylation reaction protocol. Scheme 2 reports the synthetic pathway to compounds **3c**−**g**. N^1,N^8-di-*t*-butoxycarbonylspermidine (**8**), synthesized from spermidine (**7**), was appropriately alkylated to afford products **9b**−**e**, while compound **9a**, even though its synthesis was previously reported by others,[43] was newly prepared starting from **8** by means of an acylation reaction. Compounds **9a**−**e**, after deprotection,[44] were arylated with 9-chloro-1,2,3,4-tetrahydroacridine (**4**) following a standard *N*-arylation protocol to afford the desired compounds **3c**−**g**.

The synthesis of compounds **3h**−**m** with an aryl containing spacer was accomplished as summarized in Scheme 3. For the synthesis of intermediates **12a**−**c**, we used commercially available bromides **11a**,**b** and potassium cyanide in the presence of a catalytic amount of 18-crown-6-ether in acetonitrile, while **11c**[45] was synthesized starting from **10** using a synthetic procedure employing carbon tetrabromide.[46] Alcohol **10** was obtained as previously described.[47] Compounds **12d**,**e** were commercially available. Reduction of cyano-derivative **12a** was performed with nickel chloride and sodium borohydride to afford the free base **13a**, while reduction of **12b**−**e** was carried out in the presence of Boc_2O[48] to provide the protected amines **13b**−**e**;[49] **13f** was purchased by Aldrich. Amines **13a** and **13f** and those obtained after *N*-Boc deprotection of **13b**−**e** were treated with **4** in *n*-pentanol according to a standard procedure, to afford final compounds **3h**−**m**.

Results and Discussion

3.1. Molecular Modeling, Bioinformatics Analysis, and Structure−Activity Relationship Studies (SARs). In earlier studies, we investigated the active-site gorge of AChE and BuChE by developing specific inhibitors designed to interact with different amino acids in the gorge of these enzymes.[37] The most representative compounds of the original series (**2a**−**e**, Chart 1), previously tested against fetal bovine serum (*FBS*) AChE and equine (*Eq*) BuChE, have now been tested with *h*ChEs, and results are reported in Table 1. Compound **2a** was developed[37a] to demonstrate the presence of a peripheral site at the lip of the gorge of BuChE (K_i *Eq*BuChE = 400 pM), while compounds **2b**−**e** were specifically designed to interact with different recognition sites present in the gorge of AChE and BuChE.[37b] According to our design hypothesis, the selectivity profile of **2a**−**e** was conserved when tested with *h*ChEs (Table 1). The number of protonatable functions is crucial for high inhibitory activity of AChE (K_i *h*AChE: **2b** < **2c** < **2a**, Table 1) and the introduction of a sulfur bridging atom (**2a**,**c**−**e**), which

Scheme 3. Synthesis of Compounds **13h−m**[a]

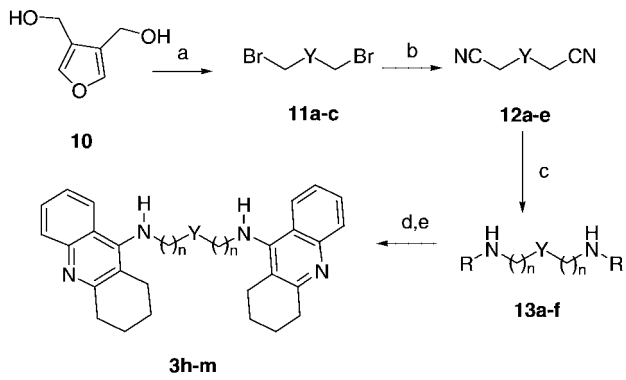

for compds **3**

	Y	n
l	5-Me-1,3-benzene	2
j	2,6-pyridine	2
m	3,4-furan	2
k	1,4-benzene	2
i	1,3-benzene	2
h	1,4-piperazine	3

for compds **11-13**

	Y	R	n
a	5-Me-1,3-benzene	H	2
b	2,6-pyridine	Boc	2
c	3,4-furan	Boc	2
d	1,4-benzene	Boc	2
e	1,3-benzene	Boc	2
f	1,4-piperazine	H	3

[a] (a) CBr_4, Ph_3P, MeCN, rt, 6 h; (b) KCN, 18-crown-6 ether, MeCN, reflux, 18 h; (c) $NiCl_2 \cdot 6H_2O$, $NaBH_4$, MeOH, rt, 4 h then water for **13a**; $NiCl_2 \cdot 6H_2O$, $NaBH_4$, Boc_2O, MeOH, rt, 18 h then diethylentriamine for **13b−e**; (d) CF_3COOH, CH_2Cl_2, rt for **13b−e**; (e) **4**, Et_3N, pentanol, 160 °C, 18 h.

reduces the protonatability of the acridine heterocyclic nitrogen (Table 1), led to a higher *h*AChE/*h*BuChE selectivity ratio (decreasing affinity for *h*AChE, e.g., **2b** vs **16**, Table 1 and Chart 2).[37] Previous docking studies[37] predicted the binding mode of the heterobivalent ligands **2a**, **2d**, and **2e** to AChE by positioning the tacrine moiety into the CAS with the thioacridine system facing the PAS, in accordance with the electronegative gradient present along the gorge of the two enzymes. Our hypothesized binding mode was recently confirmed by the resolution of the X-ray structure of compound **2a** in complex with *Tc*AChE,[50] although the unique conformational shift in W279 side chain induced by **2a** was not seen in our docking studies with *h*ChEs.

The refinement of the design strategy described herein was carried out on the basis of: (i) a thorough analysis of the X-ray crystal structures for AChEs available in the PDB, to analyze inhibitor-dependent conformational variations of AA clusters in the gorge, and (ii) a bioinformatics analysis, to verify if these inhibitor-induced conformational changes were targeting specific protein−protein interaction domains (hot spots). Consequently, we improved our docking procedure (see Refinement of Docking Parameters in the Experimental Procedures section for details) with the aim of reproducing the experimentally observed enzyme conformational shifts, which can be predictive for inhibitor potency. The results obtained for the newly designed inhibitors using the refined docking procedure were in agreement with the SAR trend observed for the synthesized compounds. This approach led to the discovery of **3d**, a novel and potent multisite inhibitor of *h*ChEs capable, as predicted by refined docking simulations, of adapting to fluctuations in enzyme hot spots (freeze-frame inhibitors). According to our hypothesis, the binding of a multisite inhibitor with a high association constant might collapse the gorge around it by cross interactions among the hot spots, while the binding of an inhibitor with a low dissociation constant might block ChE motions and functions.

3.1.a. Analysis of ChE X-ray Structures. The conformational changes present in the gorge of the 87 experimentally determined *Torpedo californica*, mouse, and human AChE X-ray crystal structures available in the PDB were calculated and tabulated. The information acquired from this structural analysis was then used to refine our dynamic docking protocol in order to optimize the dynamic simulation. In our study, we also took into account the binding mode, the inhibitory activity, and the chemical structure of the ligand in complex with AChE (Tables 1 and 2 of the Supporting Information). Accordingly, the 87 X-ray crystal structures were categorized by the source of enzyme, then classified on the basis of their binding state and the ligand binding mode (if an inhibitor was bound) (Table 1 of the Supporting Information). Conformational shifts in key residues clustered at different gorge levels, with respect to their position in the apoenzyme, were calculated (Table 2 of the Supporting Information). The *h*AChE/inhibitor complexes from our docking studies were also analyzed and classified on the same bases (Table 2 of the Supporting Information).

Taking into account the various enzyme/inhibitor complexes, upon inhibitor binding, there was a concerted movement of specific residues as depicted in Figure 1A−D, (i.e., CAS: Y337; mid gorge: D74 and Y341; PAS: W286; *h*AChE numbering). Our results also revealed that conformational changes of the enzyme always seemed to involve the same key AA clusters, and were related to inhibitor potency and binding mode (Tables 1 and 2 of the Supporting Information).

The conformational shift in PAS Trp residues (i.e., *h*W286, *m*W286, and *Tc*W279) (Figure 1D, Table 2F of the Supporting Information) was induced by tacrine-based multisite inhibitors (PDB: 2CEK, 2CKM, and 1ODC) and reactivators (PDB: 1GYU, 1GYV, and GYW). The conformational shifts in W286 (dihedral angle variations are listed in Table 2F of the Supporting Information) observed in enzyme/inhibitor complexes could be divided into two groups. One group includes the structures of *Tc*AChE in complex with low nanomolar tacrine-based heterobivalent ligands such as **2a** (PDB: 2CEK) and tacrine homo- and heterodimers (PDB: 2CKM and 1ODC). The other group is represented by the unique conformational shift induced by the femtomolar click-chemistry engineered inhibitor syn-TZ2PA6 in complex with mouse AChE (*m*AChE, PDB: 1Q83).[38] From these data, there appears to be a relationship between potency and inhibitor-induced conformational shifts in Trp at the PAS. Accordingly, while the potency of the homobivalent ligand **14** (Chart 2; PDB: 2CMF, Table 1 of the Supporting Information) was 20 times lower than that of its 7-methylene counterpart **15** (Chart 2; PDB: CKM, Table 1 of the Supporting Information),[51] the analysis of the structures of these two homobivalent tacrine-based ligands[51] in complex with *Tc*AChE revealed a superimposable binding mode at the CAS and interactions with the same cluster of AA at the PAS (W286, Y124, and Y72, *h*AChE numbering). Nevertheless, only the more potent analogue **15** induced a significant conformational shift in W286 with respect to the apoenzyme, as mentioned above. This conformational shift was associated with a charge-assisted $\pi-\pi$ interaction between the tetrahydroacridine system and several aromatic rings at the PAS (i.e., triple stacking with W286 and Y72 assisted by a T-shape $\pi-\pi$ interaction with Y124) and at the CAS (W86, Y337, and Y449) of the enzyme. Analogously, the highly potent inhibitors of *m*AChE *syn*-TZ2PA6 and anti-TZ2PA6, although displaying a similar interaction pattern with the enzyme (PDB: 1Q83 and 1Q84), strikingly differ in the conformational shift in W286. Indeed, the interactions established by syn-TZ2PA6 with W286, Y72 (triple stacking), and Y124 at the PAS, strongly contribute to the tightest binding of the syn isomer with the enzyme (*syn*-

Table 1. Dissociation Constants for the Inhibition of *h*AChE and *h*BuChE by Tacrine-Related Compounds **3a**−**m** and Reference Compounds

		% prot[a]			*K*i (pM) (±SEM)		
compd	tether	mono	di	tri	*h*AChE[b]	*h*BuChE[b]	*h*AChE/*h*BuChE ratio
1					36000 (1000)	7000 (2000)	5.14
2a	$NH(CH_2)_8S$	92	6		27950 (2420)	1650 (100)	16.9
2b	NH-3-N(Me)-3-NH	0	4	96	540 (29)	12130 (1600)	0.04
2c	NH-3-N(COMe)-3-S	93	6		13370 (1600)	3130 (390)	4.27
2d	NH-3-N(Me)-4-S	2	92	6	3990 (270)	8590 (540)	0.46
2e	NH-3-N(COMe)-4-S	93	6		5150 (170)	740 (100)	6.96
3a	NH-4-N(COMe)-3-S	89	5		20877 (2075)	270 (32)	77.04
3b	NH-4-NH-3-S	7	89	4	2672 (617)	779 (77)	3.42
3c	NH-3-N(COMe)-4-NH	13	87		223 (55)	725 (260)	0.34
3d	NH-3-N(Me)-4-NH	1	14	85	11.8 (1.2)	819 (112)	0.01
3e	NH-3-N(Et)-4-NH	1	14	85	162 (41)	435 (31)	0.37
3f	NH-3-N(allyl)-4-NH	1	17	82	84.7 (16.8)	4191 (414)	0.02
3g	NH-3-N(βOHEt)-4-NH	1	17	82	119.1 (31.8)	1187 (203)	0.10
3h	NH-3-Pip-3-NH	5	42	53	135.9 (19.3)	3223 (323)	0.03
3i	NH-2-(1,3-Ph)-2-NH	3	97		1718 (390)	924 (125)	1.86
3j	NH-2-(2,6-Pyr)-2-NH	4	94	1	768 (115)	1872 (365)	0.41
3k	NH-2-(1,4-Ph)-2-NH	3	97		1630 (290)	13860 (1170)	0.12
3l	NH-2-(1,3-(5-MePh))-2-NH	19	81		7450 (580)	5040 (470)	1.48
3m	NH-2-(3,4-furan)-2-NH	3	97		13270 (3140)	7290 (860)	1.82
15					1300 (100)[c]	2000 (500)[d]	0.65[e]
16					9100 (1000)[c]	4200 (800)[d]	2.17[e]

[a] Apparent pK_a values were calculated using ACD/pK_a DB 10.0 software, (Advanced Chemistry Development Inc., Toronto, Canada) [b] K_i is the mean of at least three determinations. [c] K_i for *FBS*AChE is from ref 37. [d] K_i for *Eq*BuChE is from ref 37. [e] *FBS*AChE/*Eq*BuChE.

Chart 2. Chemical Structures of Compounds **14**−**16**

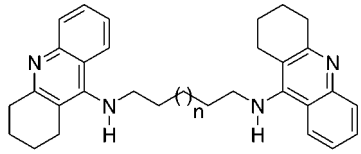

14, n = 1
15, n = 3

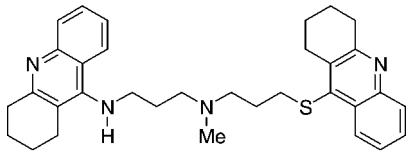

16

TZ2PA6 is 20 times more potent than its *anti* isomer). Finally, in some cases, inhibitor binding at the CAS induced conformational shifts at the PAS and vice versa, thus confirming the presence of concerted fluctuations for specific CAS and PAS substructures and highlighting the importance of mutual allosteric modulation of CAS/PAS in the function of AChE. Indeed, the interaction of CAS inhibitor tacrine (PDB: 1ACJ) with F330 (Y337 in *h*AChE), allosterically induced a conformational shift in PAS Trp residue (Figure 1A,D, Table 2F,G of the Supporting Information); on the other hand, the peripheral-site ligands, fasciculin (PDB: 1FSS and 1B41) and gallamine (PDB: 1N5M) induced a conformational shift in Y337 and W86, respectively (Figure 1A and Table 2G of the Supporting Information).

3.1.b. Bioinformatics Analysis: Identification of Protein Hot Spots. ChEs are composed of domains involved in catalytic and noncatalytic functions,[52] and an increasing number of evidence indicates the crucial role played by both inter- and intramolecular protein−protein interactions in these functions. Protein−protein interactions involve an apparent complementarity between the two surfaces, which requires a certain degree of flexibility and adaptivity in protein structure. Indeed, intrinsic fluctuations in protein structure may cause a switch in interaction between complementary hot spots.[35] The ability to predict "a priori" these binding sites (hot spots) would restrict the conformational search in the design of new leads to interfere with specific protein functions.

We performed a bioinformatics analysis of *h*AChE and *h*BuChE structures with the aim of identifying protein−protein interaction domains in terms of linear motif and/or structural elements that could contribute to the architecture of the active-site gorge and drive the motions/function of this family of enzymes (see the Experimental Section for details). We identified several hydrophobic AA clusters, similar in terms of composition (ConSeq)[53] and relative position (i.e., Cα and side chain centroid distances; Tables 3 and 4 of the Supporting Information) to the interaction residues belonging to Src-homology 3 (SH3) domain[54–56] and LxxLL motif[57–60] known to regulate an array of protein conformation/function by inter- and intramolecular protein−protein interactions. The identified residues are listed in Tables 3 and 4 of the Supporting Information, while some of the most relevant protein−protein interaction domains are depicted in Figure 2A,B. These hydrophobic clusters belong to different enzyme substructures and cooperate to ensure protein functioning (opening and closing of the gorge, enzyme breathing), thus representing protein hot spots responsible for fluctuation/function in *h*ChEs. These domains are generated by the mutual arrangement of other protein−protein interaction domains participating in the gorge architecture and sharing analogous structural features (Table 2, Figure 2A,B and Tables 3 and 4 of the Supporting Information).

In particular, in the catalytic-Glu region of *h*AChE (Figure 2A, white) we identified the ^{337}YFLVY^{341} sequence which can be "read" as an LxxLL-like motif in both parallel and antiparallel directions, thus being able to interact either with the inverted LxxLL-like motif ^{76}LYPGF^{80} in the D74 Ω-loop (Figure 2A, orange) or with the LxxLL-like motif ^{451}IEFIF^{455} present in the catalytic-His region (Figure 2A, magenta). Indeed, L76 (^{76}LYPGF^{80}) establishes hydrophobic interactions with Y341 and V340 (centroid distances of 4.67 and 5.85 Å, respectively) present in ^{337}YFLVY^{341}. On the other hand, F80 interacts through a T-shape $\pi-\pi$ interaction with W439 (catalytic-His

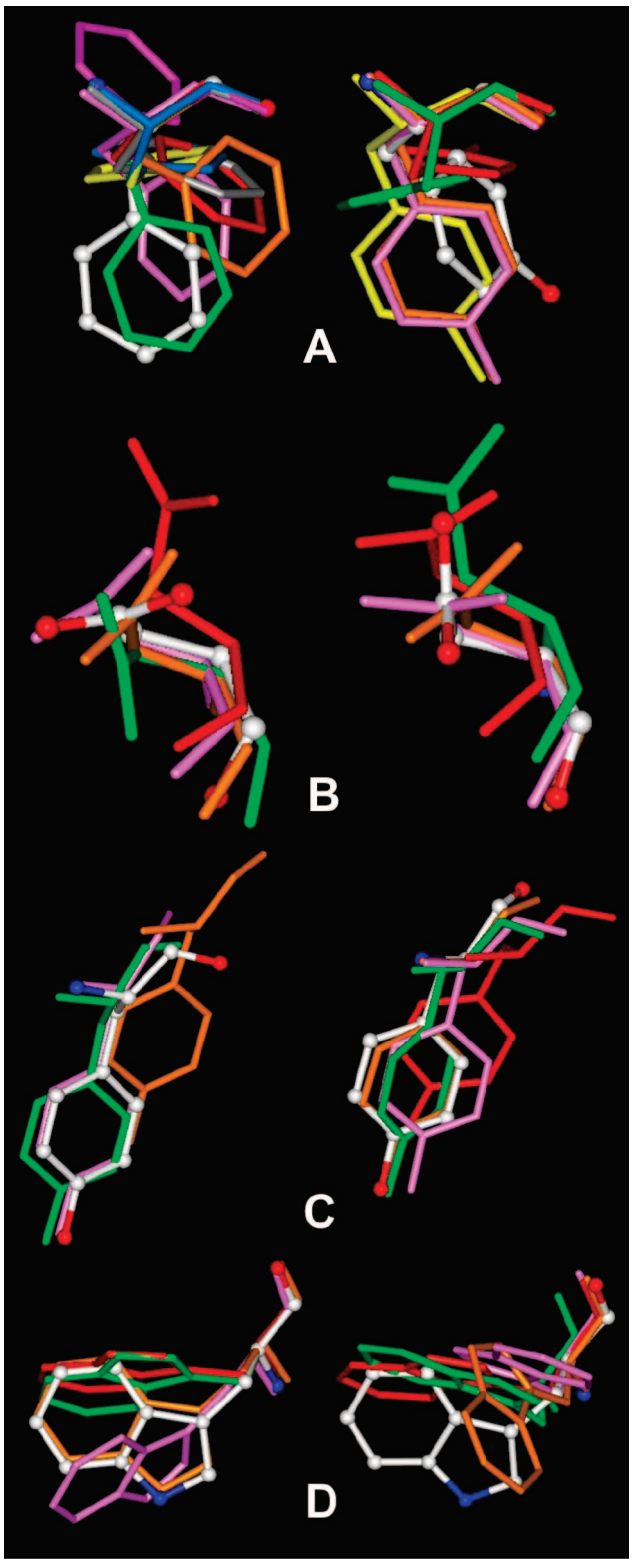

Figure 1. Conformational shifts observed in the X-ray structures of *Tc*AChE (left) and *m*AChE/*h*AChE (right). (A) Y337, (B) D74, (C) Y341, and (D) W286 (*h*AChE numbering). Reference structures 1EA5 (*Tc*AChE) and 1J06 (*m*AChE) are displayed in ball and sticks and colored by atom type. Other residues are colored according to the family reported in Table 2 of the Supporting Information, not all residues present the same number of families. Pink: family 2/B; orange: family 3/C; green: family 4/D; red: family 5/E; blue: family 6/F; grey: family 7/G; yellow: family 8/H; magenta: family 9. Numbers: *Tc*AChE families; letters: *m*AChE/*h*AChE family.

region), thus generating an aromatic (SH3-like) interaction cluster constituted by W439, Y77, and F80 (Figure 2A, Table 3 of the Supporting Information). The interactions between these AA clusters play a critical role in the functioning of *h*AChE, with the D74 Ω-loop (69−96) involved in the CAS/PAS allosteric modulation (breathing mechanism). On the basis of our analysis, two main functional hot spots were located in the active-site gorge of *h*AChE (Figure 2A white circles; Tables 3 and 4 of the Supporting Information): at the CAS represented by W86 (Ω-loop), Y337 (catalytic-Glu region), and Y449 (catalytic-His region), and at the PAS represented by Y341 (catalytic-Glu region), W286 (PAS), Y124 (Gly wall), and Y72 (Ω-loop). The structural/functional connection between these hot spots are modulated by D74 interactions and/or movements, driven by fluctuations in the LxxLL motif ^{76}LYPGF^{80} (Ω-loop) and in Y341 (^{337}YFLVY^{341}). In *h*BuChE, the corresponding Ω-loop (65−92) does not play the same functional role even though the Asp residue (D70) is conserved. Accordingly, we did not identify any LxxLL-like motif on the Ω-loop of *h*BuChE (part A vs part B of Figure 2A–D, Table 4A,C of the Supporting Information). Indeed, as reported in Figure 2B and Table 4 of the Supporting Information, in *h*BuChE, we could identify LxxLL-like motifs only in the catalytic-His region and in the peripheral site. In addition, as reported in Figure 2C,D, the AA motions resulting from our dynamic docking analysis were quite different in *h*AChE and *h*BuChE. For example, in *h*AChE, we observed a significant fluctuation of the Ω-loop C69−C96; in particular, D74 could establish charge-assisted hydrogen bond contacts with several Tyr residues which are part of CAS (W86, Y449, and Y337) or PAS (Y341, W286, Y72, and Y124) hot spots. The interaction between D74 and the Tyr network could drive the CAS/PAS mutual allosteric modulation, allowing conformational changes that contribute to AChE fluctuations and function. It is noteworthy that three of five Tyr residues are not conserved in the active-site gorge of *h*BuChE. This fact was confirmed by targeting D74 by an extra protonatable function (**2b**)[37b] that strongly increased inhibitory potency toward *h*AChE (**2b** vs **15**, Chart 2, Table 1), while the specific targeting of D70 in *h*BuChE did not provide the same increment in inhibitory potency (**2b** vs **15**, Table 1).

In summary, we identified AA clusters which are either implicated in active-site gorge fluctuation/function (Figure 1A–D, and Tables 1 and 2 of the Supporting Information) or involved in protein−protein interactions known to be crucial for inhibitor binding (Figure 2A–D, and Tables 3 and 4 of the Supporting Information). Therefore, we hypothesized that these residues represent flexible protein hot spots whose relative positioning drives the functional/conformational switch of the enzyme and that the conformational shift in hot spots, induced by inhibitor binding, may be predictive of inhibitor potency. On these bases, we designed picomolar inhibitors of *h*ChEs, which are characterized by different selectivity profiles for *h*AChE and *h*BuChE.

3.1.c. Rational Design of Compounds 3a−m and SAR Studies. The refinement of our design strategy, as described above, led to the development of a new series of tacrine-based multisite inhibitors (**3a−m**, Chart 1). As predicted by the results of our computational studies, the nature and the length of the spacer connecting the moieties binding specific hot spots modulate inhibitor potency and selectivity (Table 1).

Previous SAR studies[51] with tacrine homodimers demonstrated that the bis(7)-tacrine homodimer (**15**, Chart 2) was the optimally spaced AChE inhibitor as it formed favorable sandwich-type stacking interactions at both the CAS and the PAS. We successively discovered that introduction of an extra interaction point at the tether level could improve the inhibitory activity of **15** (**2b** vs **15**). We hypothesized that the potency of

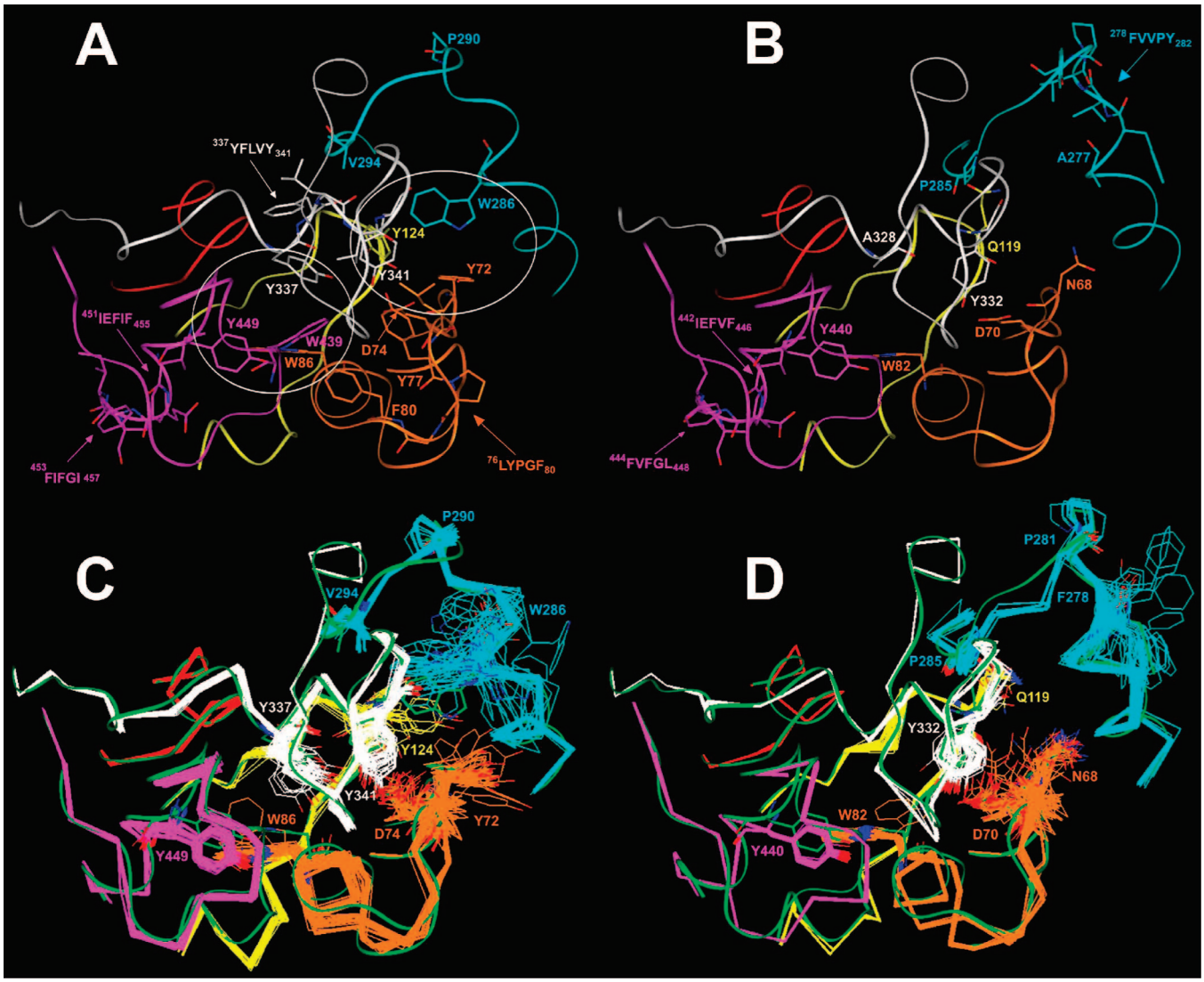

Figure 2. Substructures of active-site gorges in *h*AChE (A; PDB: 1B41) and *h*BuChE (B; PDB: 1P0I): Ω-loop (orange); catalytic-His (magenta), -Glu (white), and -Ser regions (red); Gly wall (yellow); PAS (cyan). The putative protein−protein interaction domains are highlighted by arrows (motifs) or circles (structures). (C) Docked structures of *h*AChE in complex with compounds **3a**−**m** are superimposed (Cα atoms) on *h*AChE crystal structure (green ribbons). (D) Docked structures of *h*BuChE in complex with compounds **3a**−**m** superimposed on *h*BuChE (Cα atoms) crystal structure (green ribbons).

Table 2. *h*AChE and *h*BuChE Key Protein Substructures Constituting the Active-Site Gorge

region	*h*AChE residues	*h*BuChE residues
catalytic histidine region	429–455	420–446
catalytic glutamate region	326–359	317–350
catalytic serine region	199–209	194–204
Ω-loop region	69–96	65–92
glycine wall	117–134	112–129
PAS	279–297	270–288

these compounds could be further improved by specific modification of the tether as a function of the relative orientation of the targeted enzyme hot spots. Consequently, protein conformational fluctuations were specifically taken into consideration in the design process, especially considering the case of multifunctional enzymes such as ChEs. Accordingly, the extension of the tether linker of compound **2b** (the most potent inhibitor of *h*AChE of the original series) by just one methylene unit produced a dramatic increase in inhibitory potency and selectivity toward *h*AChE with respect to *h*BuChE (**3d**, $Ki_{h\text{AChE}}$ = 11.8 pM, $Ki_{h\text{BuChE}}$ = 819 pM and *h*AChE/*h*BuChE ratio of 0.01; Table 1). These results validated our docking studies, which indicated that, similarly to **2b**, compound **3d** interacts with the three identified recognition sites in *h*AChE (CAS, midgorge (D74), and PAS) (Figure 3A) but, in addition, **3d** has the necessary flexibility either to freeze the geometrically constrained *h*AChE active-site gorge in a closed conformation or to dynamically oppose the catalytic "breathing" of the enzyme (in particular of the flexible D74 Ω-loop, parts C and A of Figures 2 and 3). Moreover, our results evidenced how the "allosteric fluctuation" of the Ω-loop allows the possibility of two energetically affordable binding modes, which may contribute to the potency and selectivity of **3d** toward different conformational states of *h*AChE. Placing the 4-methylene chain toward CAS (Bind_1; Figure 3A, ligand green), **3d** is able to: (i) hydrogen bond with the backbone carbonyl group of G448 and establish a $\pi-\pi$ interaction with either W86 or Y337, stabilizing the "closed" conformation of the CAS hot spot, (ii) set up, through its protonated functions, a H-bond interaction network with the side chains of D74, Y337, and Y124 and a cation$-\pi$ interaction with the side chain of Y341 (LxxLL-like motif ^{337}YFLVY^{341}), driving the simultaneous binding of D74

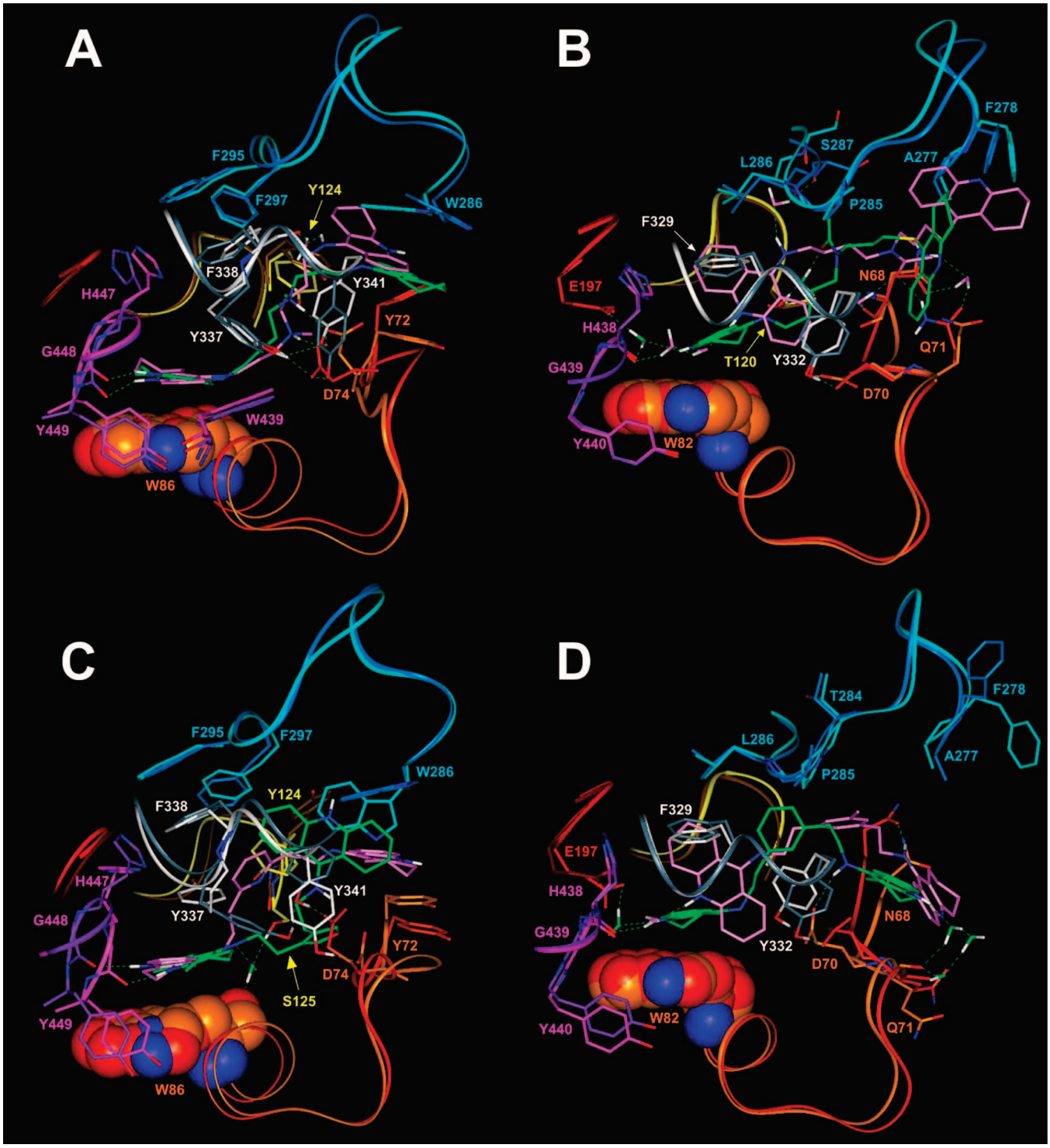

Figure 3. Substructures of active-site gorges in *h*AChE (A; PDB: 1B41) and *h*BuChE (B; PDB: 1P0I): Ω-loop (orange); catalytic- His (magenta), -Glu (white), and -Ser regions (red); Gly wall (yellow); PAS (cyan). (A) Binding modes 1 (ligand: green; protein: lighter) and 2 (ligand: pink; protein: darker) of **3d** in *h*AChE superimposed by Cα atoms. VdW volume of W86 are displayed. (B) Docked complexes of **3a**/*h*BuChE in binding modes 1 (ligand: green; protein: lighter) and 2 (ligand: pink; protein: darker) superimposed by Cα atoms. VdW volume of W82 is displayed. (C) Docked complexes of **3j**/*h*AChE (ligand: pink; protein: darker) and **3m**/*h*AChE (ligand: green; protein: lighter) superimposed by Cα atoms. VdW volume of W86 is displayed. (D) Docked complexes of **3i**/*h*BuChE (ligand: green; protein: lighter) and **3l**/*h*BuChE (ligand: pink; protein: darker) superimposed by Cα atoms. VdW volume of W82 is displayed. All heteroatoms are colored by atom type (O = red; N = blue). Hydrogen bonds are highlighted by green dashed lines. Hydrogens (white) and water molecules are omitted for clarity, except those involved in hydrogen bond interactions.

(Ω-loop) to Y337 (CAS) and to Y341 and Y124 (PAS), and (iii) establish a triple $\pi-\pi$ stacking with W286 and Y72, thus inducing a rotation of W286 side chain toward the aromatic group of Y124 (121°, Table 2F of the Supporting Information) and enforcing the PAS hot spot interactions (W286−Y72−Y124; Figure 3A). It is noteworthy that **3d** can also achieve a similar interaction pattern, characterized by an equivalent interaction energy, by placing the 4-methylene chain toward PAS (Bind_2; Figure 3A, ligand pink, Table 5 of the Supporting Information). To prove the role of the fluctuation of *h*AChE Ω-loop (D74),

we increased the length of the alkyl tether of the thioacridine series of bivalent multisite ligands by one methylene unit, either at the tetrahydroacridine side (**3b**, facing the CAS) or at the thioacridine side (**2d**, facing the PAS).[37,50] According to our computational results, the inhibitory activity of the compounds bearing an extra protonatable function at the tether level (Chart 1) toward *h*AChE was improved in both cases (**2d** and **3b** vs **16**, Charts 1,2 and Table 1). On the contrary, the same set of compounds showed a different rank order of potency with *h*BuChE (**3b** > **16** > **2d**, Table 1), consistent with the predicted placement of the Ω-loop closer to the PAS than to the CAS (Figure 2C,D). Consequently, the activity profile of these newly designed compounds with *h*ChEs validates our design strategy which exploits the calculated enzyme fluctuations together with the results of bioinformatics analysis for drug design.

In line with our hypothesis, a completely different AChE activity trend was obtained in the thioacridine series when the protonatable function at the tether level was replaced by an *N*-acetyl group in order to abolish the ionic interaction with the Asp residue in the Ω-loop, thus targeting other midgorge hot spots. Indeed, **3a** (NH-4-N(COMe)-3-S) showed a lower affinity for *h*AChE, compared to both **2e** (NH-3-N(COMe)-4-S) and its inferior homologue **2c** (NH-3-N(COMe)-3-S) (Table 1). On the contrary, the activity trend was confirmed with BuChE: **3a** proved to be more potent than **2e** and **2c** (Table 1). Interestingly, due to the larger and less flexible gorge of *h*BuChE, our docking results predicted two energetically comparable binding modes for compound **3a** (Table 5 of the Supporting Information), which interact either with the CAS and the midgorge recognition site (Figure 3B, ligand green and Table 5B of the Supporting Information, Bind_1) or with the midgorge recognition site and the peripheral site (Figure 3B, ligand pink and Table 5B of the Supporting Information, Bind_2). In the CAS/midgorge binding mode in *h*BuChE (Figure 3B, ligand green), the linker NH-4-N(COMe)-3-S allows compound **3a** to establish a 2-fold stronger $\pi-\pi$ interaction with the side chain of W82 with respect to compound **2e** (Table 5 of the Supporting Information). On the other hand, the midgorge/peripheral site binding mode of **3a** (Figure 3B, ligand pink), is characterized by tighter interactions with F278 (^{278}FVVPY^{282} motif, Figure 2B) and Q71 than those calculated for **2e** (Table 5 of the Supporting Information). The existence of two possible energetically comparable binding modes for compound **3a** might also be due to the replacement in *h*BuChE of Y337 (*h*AChE) by Ala (A328), which results in the loss of a specific hydrophobic anchor domain and consequently of a triple stacking interaction with the tacrine moiety of the ligand (Figure 3A, B). Thus, our docking results indicated that, similarly to **3d** in complex with *h*AChE, the binding of **3a** to *h*BuChE was entropically favored. Accordingly, **3a** resulted the most potent and selective *h*BuChEI of the series ($Ki_{h\text{BuChE}}$ = 270 pM, *h*AChE/*h*BuChE ratio of 77, Table 1).

Because of the lack of the protonatable function at the spacer level, compound **3a** is unable to enforce the D74 hot spot interactions with the Tyr network (^{337}YFLVY^{341} at CAS, and Y124 at PAS) in *h*AChE, thus resulting in a potency that is 1 order of magnitude lower than **3b**.

Replacement of the thioacridine moiety of **3a** by tacrine (**3c**, NH-4-N(COMe)-3-NH) reversed the affinity profile of the ligand, making **3c** 100-fold more potent than **3a** for *h*AChE while slightly lowering its affinity for *h*BuChE (Table 1). The more hydrophobic thioacridine moiety of **3a** interacts better with the peripheral site of *h*BuChE (F278 at ^{278}FVVPY^{282} motif),[37,50] while the presence of the second tacrine moiety allows **3c** to strongly interact with W286 of *h*AChE, through a cation$-\pi$ stacking. It is noteworthy that, despite the presence of a second protonatable moiety, **3c** (NH-4-N(COMe)-3-NH) was still as active as **2e** (NH-3-N(COMe)-4-S) toward *h*BuChE because, similar to **3a**, it was able to place the 4-methylene linker toward the CAS.

The effect of different *N*-alkyl/alkenyl chains on the potency and selectivity of inhibitors was evaluated through the synthesis of the **3d**-homologous multisite ligands **3e**−**g** (*N*-Et, **3e**; *N*-allyl, **3f**; *N*-β-OHEt, **3g**). As previously reported, there are key AA residues in the active-site gorge of *h*ChEs which affect: (i) the electronegative gradient along the gorge (*h*AChE > *h*BuChE), (ii) the shape and void of the gorge, and (iii) the fluctuation of the enzyme through different conformational states (*h*AChE > *h*BuChE). The crucial differences at the midgorge and peripheral sites between *h*BuChE and *h*AChE (e.g., *h*BuChE/*h*AChE: A277/W286, F278/H287, G283/E292, P285/V294, L286/F295) generate a unique LxxLL-like motif ^{278}FVVPY^{282} (part A vs part B of Figure 2) in *h*BuChE and confer a strong hydrophobic nature and a defined shape to the larger *h*BuChE gorge, which allows the accommodation of bulky but adaptable hydrophobic groups. Consequently, while the replacement of the methyl group (**3d**) by an ethyl group (**3e**) resulted in a 2-fold increase in affinity for *h*BuChE and its replacement by a β-hydroxyethyl group (**3g**) still retains high potency, the introduction of an allyl group resulted in a 10-fold drop in affinity for *h*BuChE (**3f** vs **3e**, Table 1). On the other hand, according to our bioinformatics and docking results, compound **3f** conserved an excellent inhibitory activity and a very good selectivity toward *h*AChE ($Ki_{h\text{AChE}}$ = 84.7 pM, $Ki_{h\text{BuChE}}$ = 4191 pM and *h*AChE/*h*BuChE ratio of 0.02), due to $\pi-\pi$ interactions with specific aromatic hot spots (Figure 1 of the Supporting Information). Indeed, placing the 3-methylene linker toward the CAS, compound **3f** perfectly accommodates its allyl group into the *h*AChE aromatic pocket constituted by the LxxLL-like motif ^{337}YFLVY^{341} and replaces Y337 in stacking with W86, causing the shift of Y337 side chain toward Y341 (Bind_2, Figure 1 of the Supporting Information, ligand green). This structural rearrangement assisted by a H-bond with Y124 (Gly wall) strongly enforces the Y124(PAS)-Y337(CAS)-Y341(PAS)-D74(Ω-loop) network. Furthermore, the tetrahydroacridine moiety establishes a triple stacking with W286 and Y72 at the PAS. The simultaneous interaction of **3f** with Y341, Y124, Y72, and W286 determines the closure of the PAS hot spot around the ligand. In addition, the presence of multiple aromatic hot spots along the *h*AChE gorge (Table 3 of the Supporting Information) and the fluctuations of the D74 Ω-loop allow a further energetically achievable binding mode for **3f** by placing the 4-methylene linker toward the PAS (Bind_1, Figure 1 of the Supporting Information, ligand pink, and Table 5 of the Supporting Information).

To (i) further evaluate the presence and the function of fluctuating functional hot spots in *h*AChE active gorge and (ii) confirm the key role played by the mutual adaptability of the protein and ligand structures in enzyme binding and inhibition, a N^1,N^4-bis(3-aminopropyl)piperazine linker was introduced at the tether level in the bis-tacrine series (**3h**, Table 1). Indeed, calculations of pK_a values indicated that, at physiological pH, only one piperazine nitrogen was protonated although the single pK_a value of the two tertiary amine functions was identical (7.03 ± 0.70). Dynamic docking studies with *h*AChE highlighted the possibility for **3h** to establish favorable cross interactions with D74 (Ω-loop) and the Tyr network present at the gorge hot spots, positioning the protonated piperazine nitrogen closer either to the CAS or to the PAS (Bind_1 and Bind_2, respectively;

Figure 2 and Table 5 of the Supporting Information). Therefore, the presence of two adjacent binding sites (CAS and PAS hot spots, Figure 2A) for the cationic substrate ACh (allosterically modulated by the fluctuation of D74 Ω-loop) favors the interaction between *h*AChE active site gorge and **3h**, similar to **3d** and **3f**. The activity profile of **3h** supported these results, being that this compound is extremely potent and selective for *h*AChE (Ki_{hAChE} = 135.9 pM, Table 1).

We also investigated the effect on selectivity and potency of a protonatable nitrogen in alkylarylalkyl tethers (**3i**−**m**). In general, compounds **3i**−**m** showed lower potencies against *h*AChE compared to the spermidine analogues **3d**−**g** while maintaining the affinity for *h*BuChE in the nanomolar range, which resulted in a selectivity ratio of 0.12−1.86. This SAR trend further outlines the predicted importance of ligand conformational flexibility for interaction with *h*AChE. The presence of the basic pyridine ring at the tether level of **3j** is responsible for high activity and selectivity toward *h*AChE (Table 1). Indeed, although not protonated at physiological pH (Table 1), the pyridine nitrogen is a soft Lewis base able to interfere with the hydrogen bond network present in *h*AChE active site gorge. Accordingly, results of docking studies on the **3j**/*h*AChE complex (Figure 3C, ligand pink) indicated the presence of an H-bond interaction with S125 side chain (distance < 3 Å) and a rearrangement of the catalytic Glu region (Y337 and Y441) with respect to the D74 Ω-loop. Indeed, although the docked complex reported in Figure 3C showed that the position of the pyridine nitrogen of **3j** overlaps the protonated nitrogen of **3d** in one of the two possible binding modes (Figure 3A, ligand green), the position of D74 Ω-loop markedly differs in the two complexes (part A vs part C of Figure 3) due to the lack of an ionic interaction with the pyridine nitrogen. In agreement with our docking results, the lack of a protonated nitrogen and the limited structural adaptability of **3j** resulted in a 65-fold decreased potency with respect to **3d**.

The selectivity profile was reversed when the spacer was substituted by a (1,3-phenylene)diethanamine, with **3i** being slightly more potent toward *h*BuChE than *h*AChE (Ki_{hAChE} = 1718 pM, Ki_{hBuChE} = 924 pM). The affinity for *h*BuChE decreased when the meta-branched phenyl of **3i** was replaced by a para-substituted phenyl ring (**3k**, Ki_{hBuChE} = 13860 pM). As discussed above, we hypothesized that the replacement of key AAs in the *h*BuChE gorge accounts for the lower degree of conformational flexibility of the active-site gorge of this enzyme compared to *h*AChE (Figure 2B, D). In particular, the close proximity of *h*BuChE P285 to the SH3-like aromatic cluster formed by F329 and Y332 (Table 3C of the Supporting Information) in the catalytic-Glu region, and to W430 in the catalytic-His region confers conformational rigidity to this narrow hinge of the gorge. As evidenced in Figure 3D (ligand green), the 1,3-disubstituted phenyl ring of **3i** (Ki_{hBuChE} = 924 pM) is able to adapt to this site of the enzyme by: (i) interacting with F329 and Y332, (ii) maintaining a good $\pi-\pi$ stacking with W82 (CAS), and (iii) establishing a H-bond with D70 (Ω-loop). On the other hand, the para-branched phenyl of **3k** (Ki_{hBuChE} = 13860 pM) and the methyl-substituted phenyl ring of **3l** (Ki_{hBuChE} = 5040 pM) (Figure 3D, ligand pink) do not fit in this region of the enzyme, shifting the ligand toward the PAS and reducing its interaction with the CAS residues.

In contrast, we observed a different SAR trend toward *h*AChE for the aryl-tethered compounds (**3i**, **3k**, and **3l**, Table 1), in agreement with the highlighted presence of multiple aromatic hot spots along the *h*AChE gorge as well as with its higher degree of conformational flexibility (Figure 2A−D). According to our docking results, due to the stronger polarization of *h*AChE active-site gorge, the potency of the ligand was mostly affected by changing the electronic properties of the aromatic tether. As depicted in Figure 3C and reported in Table 2F of the Supporting Information, the results of docking studies with compound **3m** in *h*AChE showed the displacement of the D74 Ω-loop and the stabilization of the apo (native) position of W286 side chain. In fact, the introduction of a furane ring (**3m**) led to a 17-fold decrease in the affinity for *h*AChE compared to **3j** (Table 1 and Figure 3C). As expected, the electronegative nature of the furane ring does not match the electronegative potential present along the active-site gorge of the two enzymes and the inhibitory activity decreases according to the difference in the electronegative gradient between *h*AChE and *h*BuChE gorges (*h*AChE > *h*BuChE).

Conclusions

The observation that conformational fluctuations play an important role in protein function suggests that functional residues may be uniquely coupled to structural fluctuations.

In both families of *h*ChEs, we identified specific hot spots, responsible for protein fluctuations and functions, and those active-site residues that play a role in modulating the cooperative network between the key substructures, in order to exploit this information for rational drug design.

Thus, to develop novel and extremely potent inhibitors of *h*AChE and *h*BuChE for modulating their classical and nonclassical functions, we performed a thorough bioinformatics analysis aimed at identifying protein−protein interaction domains in *h*ChEs. Through this approach, we defined several putative protein hot spots in the active-site gorges of *h*ChEs, characterized by different functional and conformational features, as key small molecule targets. Furthermore, we optimized our design strategy and dynamic docking procedure through the analysis of enzyme structures and motions. All the X-ray structures of AChEs available in the PDB were used for calculating significant conformational shifts in key residues located in different regions of the gorge, upon complexation with an inhibitor. We demonstrated that a concerted movement of specific AChE residues occurred (i.e., CAS: Y337; mid gorge: D74 and Y341; PAS: W286) upon binding of an inhibitor, and these conformational changes may be related to inhibitor potency and binding mode. In particular, there was a relationship between potency and inhibitor-induced conformational shifts in Trp at the PAS. These results led to the implementation of our design strategy of targeting identified hot spots for the development of a series of extremely potent and highly flexible reversible inhibitors characterized by *K*i values in the high to low picomolar range. In particular, compound **3d** was found to be the most potent and selective inhibitor of *h*AChE known to date (Ki_{hAChE} = 11.8 pM, Ki_{hBuChE} = 819 pM; *h*AChE/*h*BuChE ratio = 0.01). This approach of designing small molecule modulators by targeting protein−protein interaction domains may pave the way for the development of selective inhibitors toward nonclassical functions of *h*ChEs.

Experimental Procedures

Reagents were purchased from Sigma-Aldrich and were used as received. Reaction progress was monitored by TLC using Merck silica gel 60 F_{254} (0.040−0.063 mm) with detection by UV. Merck silica gel 60 (0.040−0.063 mm) was used for column chromatography. Melting points were determined using an Electrothermal 8103 apparatus. IR spectra were taken with Perkin-Elmer 398 and FT 1600 spectrophotometers. ^{1}H NMR spectra were recorded on Brüker 200 and 400 MHz and Varian 300 MHz spectrometers; the

values of chemical shifts (δ) are given in ppm and coupling constants (J) in Hertz (Hz). Splitting patterns are described as singlet (s), doublet (d), triplet (t), quartet (q), and broad (br). ^{13}C NMR spectra were recorded on Varian 300 MHz spectrometer with TMS as an internal standard. In the case of overlapping carbons, further NMR experiments were performed (e.g., HSQC and Dept analysis), and number of overlapping carbons are reported in brackets. All reactions were carried out in an argon atmosphere. Flash chromatography purifications were performed using Merck silica gel 230−400 mesh. GC-MS were performed on a Saturn 3 (Varian) or Saturn 2000 (Varian) GC-MS System using a Chrompack DB5 capillary column (30 m × 0.25 mm i. d.; 0.25 μm film thickness). Mass spectra were recorded using a VG 70-250S spectrometer. FAB-MS spectra were performed using a VG 70-250S spectrometer. ESI-MS, APCI-MS spectra were performed by an Agilent 1100 Series LC/MSD spectrometer and by LCQDeca-THERMOFINNIGAN spectrometer. Elemental analyses were performed on a Perkin-Elmer 240 °C elemental analyzer, and the results were within ± 0.4% of the theoretical values. Yields refer to purified products and are not optimized.

For testing, compounds **3a**−**m** were transformed into the corresponding hydrochloride salts by a standard procedure.

***N*-(1,2,3,4-Tetrahydroacridin-9-yl)-1,4-butanediamine**[40] **(5).** To a solution of palladium acetate (7.2 mg, 0.03 mmol) and (±)-BINAP (21.4 mg, 0.03 mmol) in freshly distilled dry dioxane (15 mL), potassium carbonate (4.458 g, 32.26 mmol), 9-chloro-1,2,3,4-tetrahydroacridine (**4**) (0.350 g, 1.61 mmol), and 1,4-diaminobutane (194 μL, 1.93 mmol) were added. The reaction was refluxed in argon atmosphere for 12 h. Then, the solvent was removed under reduced pressure, water was added, and the water phase was extracted with ethyl acetate (3 × 30 mL). The organic layers were combined, dried over Na_2SO_4, filtered, and evaporated. The crude product was purified by means of flash chromatography (ethyl acetate/methanol/TEA 9:1:1). Pure title compound was obtained as a yellow oil with a yield of 40%. ^{1}H NMR ($CDCl_3$) (200 MHz) δ: 1.54 (m, 2H), 1.65 (m, 2H), 1.89 (m, 4H), 1.96 (m, 2H), 2.03 (br s, 2H), 2.69 (m, 2H), 3.03 (m, 2H), 3.47 (t, 2H, J = 6.8 Hz), 4.59 (br s, 1H) 7.30 (t, 1H, J = 7.8 Hz), 7.51 (t, 1H, J = 7.1 Hz), 7.84−7.94 (m, 2H). ESI-MS m/z: 270 $[M + H]^+$ (100) 199. ESI-MS/MS of 270 $[M + H]^+$: 253, 227, 199 (100). Anal. ($C_{17}H_{23}N_3 \cdot {}^1/_2H_2O$) C, H, N.

***N*-(1,2,3,4-Tetrahydroacridin-9-yl)-*N*′-(3-(1,2,3,4-tetrahydroacridin-9-ylsulfanyl)propyl)-1,4-butanediamine (3b).** To a solution of **5** (0.100 g, 0.37 mmol) in dry acetonitrile (7 mL), potassium carbonate (51.1 mg, 0.37 mmol) and 18-crown-6 ether (0.1 mol%) were added; the resulting mixture was stirred at room temperature for 1 h in argon atmosphere. Then, 9-[(3-bromopropyl)sulfanyl]-1,2,3,4-tetrahydroacridine (**6**) (124.5 mg, 0.37 mmol) was added and the reaction mixture was refluxed for 3 h. Then the solvent was removed under reduced pressure, water was added, the water phase was extracted with ethyl acetate (3 × 30 mL), and then the combined organic layers were dried over Na_2SO_4, filtered, and evaporated. The crude product was purified by means of flash chromatography (ethyl acetate/methanol/TEA 20:1:1). Pure title compound was obtained as a yellow oil with a yield of 42%. ^{1}H NMR ($CDCl_3$) (200 MHz) δ: 1.45−1.72 (m, 6H), 1.86−2.01 (m, 8H), 2.10 (br s, 1H), 2.49−2.66 (m, 6H), 2.83 (t, 2H, J = 7.3 Hz), 3.03−3.21 (m, 6H), 3.43 (t, 2H, J = 6.8 Hz), 4.62 (br s, 1H), 7.29 (t, 1H, J = 7.6 Hz), 7.43−7.61 (m, 3H), 7.86−7.98 (m, 3H), 8.44 (d, 1H, J = 8.0 Hz). ESI-MS m/z: 525 $[M + H]^+$ 263 $[M + 2H]^{2+}$/2. ESI-MS/MS of 525 $[M + H]^+$: 454, 397, 380, 342, 310, 295, 253, 216, 199 (100), 184, 171. Anal. ($C_{33}H_{40}N_4S \cdot {}^1/_4H_2O$) C, H, N.

***N*-{4-[(1,2,3, 4-Tetrahydroacridin-9-yl)amino]butyl}-*N*-{3-[(1,2,3,4-tetrahydroacridin-9-yl)sulfanyl]propyl}acetamide (3a).** To a solution of **3b** (60.0 mg, 0.11 mmol) and triethylamine (19 μL, 0.14 mmol) in dry dichloromethane (5 mL), acetyl chloride (10 μL, 0.13 mmol) was slowly added at 0 °C. The reaction mixture was then stirred for 12 h at room temperature. Water was added and the aqueous phase was separated and extracted with dichloromethane (3 × 30 mL). The combined organic layers were dried over Na_2SO_4, filtered, and evaporated. The crude product was purified by means of flash chromatography (petroleum ether 40−60 °C/ethyl acetate/TEA/methanol 6:5:2:0.5). Pure title compound was obtained as a yellow oil with a yield of 23%. ^{1}H NMR ($CDCl_3$) (200 MHz) δ: 1.53 (m, 4H), 1.68 (m, 2H), 1.85−2.08 (m, 11H), 2.65−2.79 (m, 4H), 2.96−3.31 (m, 10H), 3.43 (m, 2H), 4.60 (br s, 1H), 7.42−7.66 (m, 4H), 7.95 (m, 3H), 8.40 (m, 1H). ^{13}C NMR ($CDCl_3$) (75.2 MHz) δ: 20.4, 21.7, 21.8, 22.0 (2), 27.8, 27.9, 28.0, 28.1, 28.2, 33.2, 33.3, 43.7, 44.2, 47.8, 47.9, 115.9, 119.4, 121.7, 123.0, 124.5, 124.8, 125.4, 127.7, 127.8, 128.3, 134.7, 134.8, 139.7, 140.2, 145.7, 149.2, 158.0, 158.1, 169.2. ESI-MS m/z: 567 $[M + H]^+$ (100) 352, 253. IR ($CHCl_3$, cm^{-1}): 3250, 1628. Anal. ($C_{35}H_{42}N_4OS$) C, H, N.

***N*-(*t*-Butoxycarbonyl)-*N*′-[3-(*t*-butoxycarbonylamino)propyl]-1,4-butanediamine**[61] **(8).** A solution of KOH (20 mol%), CDI (4.465 g, 27.54 mmol), and *t*-butyl alcohol (2.040 g, 27.54 mmol) in dry toluene (140 mL), was heated at 60 °C with stirring for 3 h in argon atmosphere; then spermidine (**7**) (2.16 mL, 13.77 mmol) was added dropwise and the resulting mixture was further heated while stirring at 60 °C for 3 h. After cooling to room temperature, the solvent was evaporated and water was added. The separated water phase was extracted with dichloromethane (3 × 100 mL), and the combined organic layers were dried on Na_2SO_4, filtered, and evaporated. Compound **8** was obtained as an amorphous white solid with a quantitative yield. The product was used in the following step without further purification. Physical and spectroscopic data are consistent with those reported in the literature.

***N*-Acetyl-*N*′-(*t*-butoxycarbonyl)-*N*-[3-(*t*-butoxycarbonylamino)-propyl]-1,4-butanediamine**[43] **(9a).** A solution of **8** (0.300 g, 0.87 mmol) and dry triethylamine (145 μL, 1.04 mmol) in dry dichloromethane (10 mL) was cooled at 0 °C, then acetyl chloride (74 μL, 1,04 mmol) was added dropwise and the resulting mixture was stirred at room temperature in argon atmosphere for 18 h. Then water was added and the separated aqueous phase was extracted with dichloromethane (3 × 10 mL); the combined organic layers were dried over Na_2SO_4, filtered, and evaporated. The crude product was purified by flash chromatography (ethyl acetate/methanol, 19:1), and compound **9a** was obtained as a yellow oil with a yield of 50%. ^{1}H NMR ($CDCl_3$) (200 MHz) δ: 1.42 (m, 18H), 1.43−1.51 (m, 4H), 1.61−1.64 (m, 2H), 2.07 (s, 3H), 2.29−3.03 (m, 2H), 3.07−3.40 (m, 6H), 4.95 (br s, 1H), 5.25 (br s, 1H). ESI-MS m/z: 410 $[M + Na]^+$. ESI-MS/MS of 410 $[M + Na]^+$: 354 (100), 310, 253, 210. Anal. ($C_{19}H_{37}N_3O_5$) C, H, N.

***N*-(*t*-Butoxycarbonyl)-*N*′-[3-(*t*-butoxycarbonylamino)propyl]-*N*′-methyl-1,4-butanediamine (9b).** Compound **8** (0.300 g, 0.87 mmol) was dissolved in dry acetonitrile (10 mL), then K_2CO_3 (0.120 g, 0.87 mmol) was added and iodomethane (54 μL, 0.87 mmol) was finally added to the resulting mixture. The solution was vigorously stirred for 18 h in argon atmosphere. Then the solvent was removed and water was added; the aqueous phase was extracted with ethyl acetate (3 × 10 mL) and the combined organic layers were dried over Na_2SO_4, filtered, and evaporated. The crude was purified by means of flash chromatography (ethyl acetate/methanol, 7:3), and compound **9b** was obtained as a yellow amorphous solid with a yield of 13%. ^{1}H NMR ($CDCl_3$) (200 MHz) δ: 1.39 (m, 18H), 1.40−1.45 (m, 4H), 1.59 (t, 2H, J = 6.7 Hz), 2.12 (s, 3H), 2.25−2.39 (m, 4H), 3.02−3.19 (m, 4H), 4.91 (br s, 1H), 5.31 (br s, 1H). ESI-MS m/z: 382 $[M + Na]^+$ (100), 282. ESI-MS/MS of 382 $[M + Na]^+$: 282 (100), 182. Anal. ($C_{18}H_{37}N_3O_4$) C, H, N.

***N*-(*t*-Butoxycarbonyl)-*N*′-[3-(*t*-butoxycarbonylamino)propyl]-*N*′-ethyl-1,4-butanediamine (9c).** Compound **9c** was obtained using iodoethane as previously described for compound **9b**. After purification, the title compound was obtained as a colorless oil with a 43% yield. ^{1}H NMR ($CDCl_3$) (200 MHz) δ: 1.00 (t, 3H, J = 7.1 Hz), 1.41 (m, 18H), 1.42−1.47 (m, 4H), 1.62 (t, 2H, J = 6.6 Hz), 2.36−2.61 (m, 6H), 3.02−3.21 (m, 4H), 4.85 (br s, 1H), 5.43 (br s, 1H). ESI-MS m/z: 396 $[M + Na]^+$. ESI-MS/MS of 396 $[M + Na]^+$: 322, 296 (100), 196. Anal. ($C_{19}H_{39}N_3O_4 \cdot {}^1/_4$MeOH) C, H, N.

***N*′-Allyl-*N*-(*t*-butoxycarbonyl)-*N*′-[3-(*t*-butoxycarbonylamino)-propyl]-1,4-butanediamine (9d).** Compound **9d** was obtained using allylbromide as previously described for compound **9b**. After

purification, compound **9d** was obtained as an amorphous yellow solid with a yield of 13%. ^{1}H NMR ($CDCl_3$) (200 MHz) δ: 1.40 (m, 18H), 1.43−1.48 (m, 4H), 1.58 (t, 2H, J = 6.6 Hz), 2.34−2.46 (m, 4H), 3.00−3.17 (m, 6H), 4.82 (br s, 1H), 5.12 (t, 2H, J = 9.2 Hz), 5.33 (br s, 1H), 5.70−5.91 (m, 1H). ESI-MS *m/z*: 408 [M + Na]$^+$. ESI-MS/MS of 408 [M + Na]$^+$: 308 (100), 208. Anal. ($C_{20}H_{39}N_3O_4$) C, H, N.

***N*-(*t*-Butoxycarbonyl)-*N*′-[3-(*t*-butoxycarbonylamino)propyl]-*N*′-(2-hydroxyethyl)-1,4-butanediamine (9e).** Compound **9e** was obtained using 2-bromoethanol as previously described for compound **9b**. After purification, compound **9e** was obtained as a colorless oil with a yield of 50%. ^{1}H NMR ($CDCl_3$) (200 MHz) δ: 1.27−1.56 (m, 18H), 1.63 (m, 6H, J = 6.8 Hz), 2.40−2.69 (m, 6H), 2.82 (br s, 1H), 3.08−3.21 (m, 4H), 3.57 (t, 2H, J = 5.2 Hz), 4.74 (br s, 1H), 4.99 (br s, 1H). ESI-MS *m/z*: 412 [M + Na]$^+$. ESI-MS/MS of 412 [M + Na]$^+$ (100): 368, 312, 268, 212. Anal. ($C_{19}H_{39}N_3O_5 \cdot {}^1/_2H_2O$) C, H, N.

***N*-{4-[(1,2,3,4-Tetrahydroacridin-9-yl)amino]butyl}-*N*{3-[(1,2,3,4-tetrahydroacridin-9-yl)amino]propyl}acetamide (3c).** To a solution of **9a** (0.105 g, 0.27 mmol) in dry dichloromethane (4 mL), cooled at 0 °C, trifluoroacetic acid (75 μL, 1 mmol) was added and the mixture was stirred at room temperature for 1 h. The solvent was evaporated and diethyl ether was added and evaporated three times, then the residue was dissolved in methanolic ammonia (methanol/NH_4OH 33% in water 4:1) and the resulting mixture was stirred for 4 h. After that time, the solvent was removed under reduced pressure and the resulting yellow oil was dissolved in *n*-pentanol (500 μL) and TEA (76 μL, 0.54 mmol) and 9-chloro-1,2,3,4-tetrahydroacridine (**4**) (0.117 g, 0.540 mmol) were added to the resulting solution. The reaction mixture was heated at reflux (160 °C) for 18 h while stirring in argon atmosphere. Then the solvent was removed under reduced pressure and a 10% solution of NaOH in water was added to the crude; the resulting water phase was extracted with ethyl acetate (3 × 20 mL), and the combined organic layers were dried over Na_2SO_4, filtered, and evaporated. The crude product was purified by flash chromatography (ethyl acetate/methanol/TEA, 25:1:1), and the pure title compound was obtained as a pale-yellow oil with a yield of 12%. ^{1}H NMR ($CDCl_3$) (200 MHz) δ: 1.50−1.63 (m, 4H), 1.64−1.78 (m, 2H), 1.79−1.98 (m, 6H), 2.02 (d, 2H, J = 4.3 Hz), 2.06 (s, 3H), 2.50−2.73 (m, 6H), 2.90−3.02 (m, 4H), 3.10−3.29 (m, 2H), 3.30−3.51 (m, 4H), 5.01 (br s, 2H), 7.24−7.39 (m, 2H), 7.40−7.59 (m, 2H), 7.78−7.91 (m, 2H), 7.99 (d, 2H, J = 8.4 Hz). ^{13}C NMR ($CDCl_3$) (75.2 MHz) δ: 21.6, 22.8, 23.0, 23.2 (2), 23.3 (2), 25.2, 25.4, 26.5, 29.2, 34.1, 42.7, 45.0, 48.7, 49.0, 117.0, 120.0, 120.6, 122.3, 122.6, 122.9, 124.0, 124.2, 128.7 (2), 128.8, 129.1 (2), 147.5, 150.5 (2), 158.9 (2), 171.3. ESI-MS *m/z*: 550 [M + H]$^+$ (100), 352, 253. ESI-MS/MS of 550 [M + H]$^+$: 508, 451, 352, 280, 253 (100), 211, 184. IR ($CHCl_3$, cm^{-1}): 3361, 1629. Anal. ($C_{35}H_{43}N_5O \cdot {}^1/_4H_2O$) C, H, N.

***N*′-Methyl-*N*-(1,2,3,4-tetrahydroacridin-9-yl)-*N*′-{3-[(1,2,3,4-tetrahydroacridin-9-yl)amino]propyl}-1,4-butanediamine (3d).** Compound **3d** was obtained following the procedure described for (**3c**) using (**9b**) and refluxing for 32 h. After purification of the crude by flash chromatography (ethyl acetate/methanol/TEA, 13:1:2), compound **3d** was obtained as a pale-yellow oil with a yield of 16%. ^{1}H NMR ($CDCl_3$) (200 MHz) δ: 1.48−1.71 (m, 4H), 1.72−1.96 (m, 10H), 2.24 (s, 3H), 2.45 (m, 2H), 2.51 (m, 2H), 2.57−2.77 (m, 4H), 2.95−3.13 (m, 4H), 3.42−3.50 (m, 2H), 3.52−3.65 (m, 2H), 3.97 (br s, 1H), 4.96 (br s, 1H), 7.27 (t, 2H, J = 7.6 Hz), 7.51 (t, 2H, J = 7.6 Hz), 7.91 (t, 4H, J = 9.5 Hz). ^{13}C NMR ($CDCl_3$) (75.2 MHz) δ: 23.0 (2), 23.2, 23.3, 24.9, 25.0, 25.4, 28.3, 29.9, 34.0, 34.2, 42.6, 49.1, 49.5, 56.8, 58.0, 115.5, 116.3, 120.2, 120.5, 122.9, 123.2, 123.6, 123.9, 128.5, 128.6 (2), 128.9, 147.4, 147.6, 150.8, 151.4, 158.4, 158.7. ESI-MS *m/z*: 522 [M + H]$^+$ 239. ESI-MS/MS of 522 [M + H]$^+$: 324 (100), 310, 253, 239, 211, 183. Anal. ($C_{34}H_{43}N_5$) C, H, N.

***N*′-Ethyl-*N*-(1,2,3,4-tetrahydroacridin-9-yl)-*N*′-{3-[(1,2,3,4-tetrahydroacridin-9-yl)amino]propyl}-1,4-butanediamine (3e).** Compound **3e** was obtained following the procedure described for **3c** using **9c** and refluxing for 32 h. After purification of the crude by flash chromatography (ethyl acetate/methanol/TEA, 30:1:1), the title compound was obtained as a yellow oil with a yield of 14%. ^{1}H NMR ($CDCl_3$) (200 MHz) δ: 0.98 (t, 3H, J = 7.2 Hz), 1.42−1.71 (m, 4H), 1.73−2.03 (m, 10H), 2.43−2.57 (m, 6H), 2.58−2.77 (m, 4H), 2.95−3.13 (m, 4H), 3.43 (t, 2H, J = 6.4 Hz), 3.53 (t, 2H, J = 6.3 Hz), 3.87 (br s, 1H), 4.88 (br s, 1H), 7.19−7.40 (m, 2H), 7.50 (t, 2H, J = 8.25 Hz), 7.81−8.02 (m, 4H). ^{13}C NMR ($CDCl_3$) (75.2 MHz) δ: 11.5, 23.0 (2), 23.2, 23.3, 24.5, 25.0, 25.5, 28.6, 30.1, 34.1, 34.2, 47.7, 49.0, 49.6, 52.4, 53.4, 115.6, 116.3, 120.2, 120.5, 122.9, 123.2, 123.6, 123.9, 128.5 (2), 128.7, 129.0, 147.5, 147.7, 150.8, 151.3, 158.5, 158.7. ESI-MS *m/z*: 536 [M + H]$^+$. ESI-MS/MS of 536 [M + H]$^+$: (100), 338, 324, 284, 253, 239, 211, 184. IR ($CHCl_3$, cm^{-1}): 3290. Anal. ($C_{35}H_{45}N_5$) C, H, N.

***N*′-Allyl-*N*-(1,2,3,4-tetrahydroacridin-9-yl)-*N*′-{3-[(1,2,3,4-tetrahydroacridin-9-yl)amino]propyl}-1,4-butanediamine (3f).** Compound **3f** was obtained following the procedure described for **3c** using **9d**. The crude was purified by flash chromatography (ethyl acetate/TEA, 13:1) to afford the title compound as a pale-yellow oil with a yield of 53%. ^{1}H NMR ($CDCl_3$) (200 MHz) δ: 1.43−1.72 (m, 4H), 1.72−2.05 (m, 10H), 2.45 (t, 2H, J = 7.1 Hz), 2.55 (t, 2H, J = 6.6 Hz), 2.64−2.80 (m, 4H), 3.04−3.19 (m, 6H), 3.45 (t, 2H, J = 6.8 Hz), 3.55 (t, 2H, J = 6.5 Hz), 4.02 (br s, 1H), 4.98 (br s, 1H), 5.14 (t, 2H, J = 9.1 Hz), 5.70−5.95 (m, 1H), 7.29 (t, 2H, J = 7.6 Hz), 7.52 (t, 2H, J = 8.3 Hz), 7.93 (t, 4H, J = 8.5 Hz). ^{13}C NMR ($CDCl_3$) (75.2 MHz) δ: 22.9, 23.0, 23.2 (2), 24.4, 25.0, 25.4, 28.5, 29.9, 33.8, 34.1, 48.8, 49.5, 52.4, 53.8, 57.5, 116.3 (2), 118.3, 120.4 (2), 123.0, 123.1, 123.7, 123.9, 128.6 (2), 128.7, 128.9, 135.2, 147.4 (2) 150.9 (2), 158.6 (2). ESI-MS *m/z*: 548 [M + H]$^+$. ESI-MS/MS of 548 [M + H]$^+$ (100): 506, 350, 336, 296, 253, 239, 211, 199. IR ($CHCl_3$, cm^{-1}): 3272. Anal. ($C_{36}H_{45}N_5$) C, H, N.

***N*′-(2-Hydroxyethyl)-*N*-(1,2,3,4-tetrahydroacridin-9-yl)-*N*′-{3-[(1,2,3,4-tetrahydroacridin-9-yl)amino]propyl}-1,4-butanediamine (3g).** Compound **3g** was obtained following the procedure described for compound **3c** using **9e**. After purification of the crude by means of flash chromatography (ethyl acetate/methanol/TEA, 13:1:2), pure title compound was obtained as a brown amorphous solid with a yield of 31%. ^{1}H NMR ($CDCl_3$) (200 MHz) δ: 1.41−1.72 (m, 4H), 1.75−1.98 (m, 10H), 2.45 (t, 2H, J = 7.0 Hz), 2.53−2.58 (m, 4H), 2.62−2.74 (m, 4H), 2.98−3.10 (m, 4H), 3.38−3.60 (m, 6H), 4.45 (br s, 1H), 5.48 (br s, 2H), 7.30 (t, 2H, J = 7.3 Hz), 7.51 (t, 2H, J = 7.0 Hz), 7.89 (d, 4H, J = 8.4 Hz). ^{13}C NMR ($CDCl_3$) (75.2 MHz) δ: 22.8, 22.9, 23.2, 24.6, 25.1, 25.2, 29.3, 29.8, 29.9, 33.8, 34.0, 48.0, 49.4, 52.1, 54.1, 56.0, 59.1, 116.2, 116.3, 120.2, 120.3, 122.9 (2), 124.0, 124.1,128.4, 128.6, 128.7, 128.8, 147.0, 147.1, 151.0, 151.2, 158.3, 158.4. ESI-MS *m/z*: 552 [M + H]$^+$. ESI-MS/MS of 552 [M + H]$^+$ (100): 354, 340, 300, 253, 239, 211, 184. IR ($CHCl_3$, cm^{-1}): 3415. Anal. ($C_{35}H_{45}N_5O$) C, H, N.

3,4-bis(Bromomethyl)furan[45] (11c). To a stirred solution of 3,4-bis(hydroxylmethyl)furan (**10**) (0.600 g, 4.68 mmol) in dry acetonitrile (20 mL) triphenylphosphine (2.550 g, 11.24 mmol) was added and the mixture was stirred for 20 min. Then carbon tetrabromide (3.730 g, 11.24 mmol) was added to resulting mixture and the reaction was stirred for 6 h at room temperature under argon atmosphere. After that time, the solvent was evaporated and a 10% NaOH solution in water was added to the crude. The water phase was extracted with diethyl ether (3 × 100 mL), and the combined organic layers were dried over Na_2SO_4, filtered, and evaporated. The crude was purified by flash chromatography (petroleum ether 40−60 °C/diethyl ether 9:1) and pure title compound was obtained as a yellow oil with a yield of 60%. Physical and spectroscopic data are consistent with those reported in the literature.

3,5-bis(Cyanomethyl)toluene (12a). KCN (0.210 g, 3.24 mmol) and 18-crown-6-ether (0.1 mol %) were dissolved in dry acetonitrile (6 mL), and the resulting solution was stirred for 15 min. Then 1,3-bis(bromomethyl)-5-methylbenzene (**11a**) (0.150 g, 0.54 mmol) was added and the obtained mixture was refluxed for 18 h. The solvent was evaporated, water was added, and the aqueous phase was extracted with ethyl acetate (3 × 50 mL). The combined organic layers were dried over $NaSO_4$, filtered, and evaporated. The crude was purified by flash chromatography (ethyl acetate/*n*-

hexane 1:1) and pure title compound was obtained as a brown solid with a yield of 61%; mp: 73−75 °C. ^{1}H NMR ($CDCl_3$) (400 MHz) δ: 2.34 (s, 3H), 3.69 (s, 4H), 7.06 (s, 1H), 7.10 (s, 2H). Anal. ($C_{11}H_{10}N_2$) C, H, N.

2,6-bis(Cyanomethyl)pyridine[62] (12b). Compound **12b** was obtained following the procedure previously described for **12a**. The chromatographic purification (ethyl acetate/*n*-hexane 1:1) gave the product as an amorphous solid with a yield of 65%. Physical and spectroscopic data are consistent with those reported in the literature.

3,4-bis(Cyanomethyl)furan (12c). Compound **12c** was obtained following the procedure previously described for compound **12a** Chromatographic purification (ethyl acetate/*n*-hexane 1:1) gave pure title compound as a colorless oil with a yield of 61%. ^{1}H NMR ($CDCl_3$) (300 MHz) δ: 3.84 (s, 4H), 7.46 (s, 2H). Anal. ($C_8H_6N_2O$) C, H, N.

3,5-bis(2-Aminoethyl)toluene (13a). To a stirred solution of 3,5-bis(cyanomethyl)toluene (**12a**) (0.056 g, 0.33 mmol) in dry methanol (5 mL), cooled at 0 °C, $NiCl_2 \cdot 6H_2O$ (0.008 g, 10 mol%) was added; then $NaBH_4$ (0.170 g, 4.60 mmol) was added in small portions over 30 min. The reaction was exothermic and effervescent. The resulting reaction mixture containing a finely divided black precipitate was allowed to warm to room temperature and stirred for 4 h before adding $NaBH_4$ (0.170 g, 4.60 mmol). The mixture was allowed to stir for another 30 min before solvent evaporation. Then 2 mL of water were added to quench the reaction, and the resulting solution was filtered over Celite; methanol was removed, and the aqueous phase was extracted with ethyl acetate (3 × 15 mL). The combined organic layers were dried over $NaSO_4$, filtered, and evaporated to yield the product as yellow oil that was immediately used in the following step without further purification. ESI-MS *m/z*: 179 $[M + H]^+$ (100), 201 $[M + Na]^+$.

2,6-bis(2-*t*-Butoxycarbonylaminoethyl)pyridine (13b). To a stirred solution of 2,6-bis(cyanomethyl)pyridine (**12b**) (0.200 g, 1.27 mmol) in dry methanol (100 mL), cooled to 0 °C, Boc_2O (1.150 g, 5.09 mmol), and $NiCl_2 \cdot 6H_2O$ (30.0 mg, 10 mol%) were added. $NaBH_4$ (0.660 g, 17.83 mmol) was then added in small portions over 30 min. The reaction was exothermic and effervescent. The resulting reaction mixture containing a finely divided black precipitate was allowed to warm to room temperature and stirred for 18 h before adding diethylentriamine (274 μL, 2.60 mmol). The mixture was allowed to stir for another 30 min before solvent evaporation. The purple residue was dissolved in ethyl acetate and washed with a $NaHCO_3$ saturated solution (2 × 50 mL). The organic layer was dried over $NaSO_4$, filtered, and evaporated to give the crude which was purified by flash chromatography (ethyl acetate/*n*-hexane 6:4) to afford the title compound as a yellow solid with a yield of 65%; mp 100−102 °C. ^{1}H NMR ($CDCl_3$) (400 MHz) δ: 1.35 (s, 18H), 2.87 (t, 4H, J = 6.4 Hz), 3.43 (q, 4H, J = 5.9 Hz), 5.18 (br s, 2H), 6.92 (d, 2H, J = 7.5 Hz), 7.45 (t, 1H, J = 7.6 Hz). ESI-MS *m/z*: 388 $[M + Na]^+$ (100), 352, 253. ESI-MS/MS of 388 $[M+Na]^+$ (100): 188. Anal. ($C_{19}H_{31}N_3O_4$) C, H, N.

3,4-bis(2-*t*-Butoxycarbonylaminoethyl)furan (13c). Compound **13c** was obtained following the procedure previously described for compound **13b**. The title compound was obtained as a yellow solid and was used in the following step without further purification; yield: 84%. ^{1}H NMR ($CDCl_3$) (300 MHz) δ: 1.38 (m, 18H), 2.51 (t, 4H, J = 7.2 Hz), 3.25 (q, 4H, J = 6.6 Hz), 4.87 (br s, 2H), 7.16 (s, 2H). ESI-MS *m/z*: 377 $[M + Na]^+$.

1,4-bis(2-*t*-Butoxycarbonylaminoethyl)benzene (13d). Compound **13d** was obtained following the procedure previously described for compound **13b**.

The title compound was obtained as a yellow solid and was used in the following step without further purification; yield: 86%. ^{1}H NMR ($CDCl_3$) (400 MHz) δ: 1.42 (m, 18H), 2.75 (m, 4H), 3.35 (m, 4H), 4.50 (br s 2H), 7.11 (m, 4H). ESI-MS *m/z*: 387 $[M + Na]^+$.

1,3-bis(2-*t*-Butoxycarbonylaminoethyl)benzene (13e). Title compound was obtained following the procedure previously described for **13b** and the crude was used in the following step without further purification; yield: 78%. ^{1}H NMR ($CDCl_3$) (200 MHz) δ: 1.35 (m, 18H), 2.69 (t, 4H, J = 6.4 Hz), 3.28 (m, 4H), 4.76 (br s, 2H), 6.96 (d, 3H, J = 7.5 Hz), 7.16 (t, 1H, J = 7.6 Hz). ESI-MS *m/z*: 387 $[M + Na]^+$. ESI-MS/MS of 387 $[M+Na]^+$: 331 (100), 287, 231, 187.

1,4-bis[3-(1,2,3,4-Tetrahydroacridin-9-yl)aminopropyl]piperazine (3h). A solution of 1,4-bis(3-aminopropyl)piperazine (**13f**) (95 μL, 0.46 mmol), TEA (128 μL, 0.92 mmol), and 9-chloro-1,2,3,4-tetrahydroacridine (**4**) (0.200 g, 0.92 mmol) in *n*-pentanol (0.60 mL) was heated at 160 °C for 18 h. Then the solvent was removed under reduced pressure, and a 10% solution of NaOH in water was added. The water phase was then extracted with ethyl acetate (3 × 30 mL); combined organic layers were dried over Na_2SO_4, filtered, and evaporated. The crude was purified by flash chromatography (ethyl acetate/methanol/TEA 10:1:1). Pure title compound was obtained as a yellow solid with a yield of 4%; mp 202−203 °C. ^{1}H NMR ($CDCl_3$) (300 MHz) δ: 1.92 (m, 12H), 2.57 (m, 12H), 2.74 (m, 4H), 3.07 (m, 4H), 3.61 (m 4H), 5.22 (br s, 2H), 7.33 (t, 2H, J = 7.7 Hz), 7.55 (t, 2H, J = 7.5 Hz), 7.93 (d, 2H, J = 8.5 Hz), 8.06 (d, 2H, J = 8.2 Hz). ^{13}C NMR ($CDCl_3$) (75.2 MHz) δ: 23.0 (2), 23.2 (2), 25.9 (2), 29.9 (4), 49.2 (2), 53.8 (4), 57.9 (2), 116.0 (2), 120.4 (2), 123.3 (2), 123.7 (2), 128.5 (2), 128.6 (2), 147.4 (2), 151.5 (2), 158.5 (2). ESI-MS *m/z*: 563 $[M + H]^+$ (100), 283 $[M + 2H]^{2+}/2$. ESI-MS/MS of 563 $[M + H]^+$: 380, 365 (100), 351, 239, 211, 184. Anal. ($C_{36}H_{46}N_6$) C, H, N.

1,3-bis{[(1,2,3,4-Tetrahydroacridin-9-yl)amino]ethyl}benzene (3i). Compound **3i** was obtained following the procedure previously described for compound **3c**. The product was obtained as a yellow oil after chromatographic purification on silica gel (ethyl acetate/methanol/TEA 20:1:1); yield: 15%. ^{1}H NMR ($CDCl_3$) (200 MHz) δ: 1.23−1.85 (m, 8H), 2.48 (t, 4H, J = 5.8 Hz), 2.88 (t, 4H, J = 6.9 Hz), 3.01 (t, 4H, J = 6.0 Hz), 3.70 (t, 4H, J = 6.9 Hz), 5.60 (br s, 2H), 6.97 (s, 1H), 7.08 (d, 2H, J = 7.9 Hz), 7.26 (t, 4H, J = 7.6 Hz), 7.50 (t, 2H, J = 7.5 Hz), 7.78 (d, 2H, J = 8.5 Hz), 7.88 (d, 1H, J = 8.4 Hz). ^{13}C NMR (hydrochloride salt: D_2O) (75.2 MHz) δ: 20.0 (2), 21.0 (2), 22.9 (2), 27.6 (2), 35.3 (2), 48.5 (2), 111.6 (2), 114.6 (2), 118.1 (2), 124.3 (2), 124.6 (2), 127.8 (2), 129.1, 129.2, 132.4 (2), 136.9 (2), 138.3 (2), 150.0 (2), 155.8 (2). ESI-MS *m/z*: 527 $[M + H]^+$. ESI-MS/MS of 527 $[M + H]^+$ (100): 344, 329, 316, 211, 197, 183. Anal. ($C_{36}H_{38}N_4$)C, H, N.

2,6-bis{[(1,2,3,4-Tetrahydroacridin-9-yl)amino]ethyl}pyridine (3j). Compound **3j** was obtained using the procedure previously described for compound **3c**. The product was obtained as a yellow oil after chromatographic purification on silica gel (ethyl acetate/methanol/TEA 20:1:1); yield: 23%. ^{1}H NMR (CD_3OD) (200 MHz) δ: 1.53−1.87 (m, 8H), 2.45 (t, 4H, J = 5.9 Hz), 2.72−3.05 (m, 8H), 3.72 (t, 4H, J = 6.6 Hz), 6.93 (d, 2H, J = 7.8 Hz), 7.13−7.20 (m, 2H), 7.93−7.47 (m, 3H), 7.66 (d, 2H, J = 8.3 Hz), 7.87 (d, 2H, J = 8.1 Hz). ESI-MS 528 $[M + H]^+$. ESI-MS/MS of 527 $[M + H]^+$: 392, 330, 318 (100), 211, 183. Anal. ($C_{35}H_{37}N_5 \cdot {}^1/_4H_2O$) C, H, N.

1,4-bis{[(1,2,3,4-Tetrahydroacridin-9-yl)amino]ethyl}benzene (3k). Compound **3k** was obtained using the procedure previously described for compound **3c**. The product was obtained as a yellow oil after chromatographic purification on silica gel (ethyl acetate/methanol/TEA 20:1:1) with a yield of 13%. ^{1}H NMR ($CDCl_3$) (400 MHz) δ: 1.83 (m, 8H), 2.50 (t, 4H, J = 6.1 Hz), 2.91 (t, 4H, J = 6.9 Hz), 3.02 (t, 4H, J = 6.1 Hz), 3.75 (t, 4H, J = 6.9 Hz), 5.60 (br s, 2H), 7.14 (m, 4H), 7.29 (m, 2H), 7.53 (t, 2H, J = 8.2 Hz), 7.81 (d, 2H, J = 8.4 Hz), 7.89 (d, 2H, J = 8.4 Hz). ^{13}C NMR ($CDCl_3$) (75.2 MHz) δ: 22.9 (2), 23.2 (2), 24.8 (2), 33.9 (2), 37.3 (2), 50.4 (2), 116.3 (2), 120.3 (2), 123.0 (2), 124.0 (2), 128.6 (2), 128.8 (2), 129.4 (4), 137.1 (2), 147.2 (2), 150.8 (2), 158.4 (2). ESI-MS 527 $[M + H]^+$ (100): 264 $[M + 2H]^{2+}/2$. ESI-MS/MS of 527 $[M + H]^+$ (100): 329, 316, 211, 199. IR ($CHCl_3$, cm^{-1}); 3423. Anal. ($C_{36}H_{38}N_4$) C, H, N.

1,3-bis{[(1,2,3,4-Tetrahydroacridin-9-yl)amino]ethyl}-5-methylbenzene (3l). Compound **3l** was obtained using the procedure previously described for compound **3h**. The product was obtained as a yellow oil after chromatographic purification on silica gel (ethyl acetate/methanol/TEA 20:1:1) with a yield of 24%. ^{1}H NMR ($CDCl_3$) (200 MHz) δ: 1.82 (m, 8H), 2.28 (s, 3H), 2.50 (t, 4H, J

= 5.7 Hz), 2.85 (t, 4H, J = 6.7 Hz), 3.02 (t, 4H, J = 5.9 Hz), 3.71 (t, 4H, J = 6.6 Hz), 4.00 (br s, 2H), 6.80 (s, 1H), 6.88 (s, 2H), 7.26 (m, 2H), 7.51 (t, 2H, J = 7.1 Hz), 7.79 (d, 2H, J = 8.1 Hz), 7.89 (d, 2H, J = 8.2 Hz). ^{13}C NMR ($CDCl_3$) (75.2 MHz) δ: 21.5, 22.9 (2), 23.2 (2), 24.9 (2), 34.0 (2), 37.4 (2), 50.2 (2), 116.5 (2), 120.4 (2), 122.9 (2), 124.0 (2), 126.6, 128.3 (2), 128.6 (2), 128.7 (2), 139.0, 139.1 (2), 147.3 (2), 150.7 (2), 158.5 (2). ESI-MS *m/z*: 541 $[M + H]^+$ (100), 271 $[M + 2H]^{2+}/2$. ESI-MS/MS of 541 $[M + H]^+$ (100): 360, 343, 330, 197. Anal. ($C_{37}H_{40}N_4$) C, H, N.

3,4-bis{[(1,2,3,4-Tetrahydroacridin-9-yl)amino]ethyl}furan (3m). Compound **3m** was obtained following the procedure previously described for compound **3c**. Pure title compound was obtained as a yellow oil by flash chromatography (ethyl acetate/methanol/TEA 20:1:1) with a yield of 16%. ^{1}NMR ($CDCl_3$) (300 MHz) δ: 1.85 (m, 8H), 2.57 (m, 4H), 2.70 (t, 4H, J = 7.0 Hz), 3.05 (m, 4H), 3.68 (m, 4H), 4.45 (br s, 2H), 7.29 (m, 4H), 7.53 (m, 2H), 7.86 (d, 2H, J = 8.2 Hz), 7.94 (d, 2H, J = 8.2 Hz). ESI-MS *m/z*: 517 $[M + H]^+$ (100), 259 $[M + 2H]^{2+}/2$. ESI-MS/MS of 517 $[M + H]^+$: 319(100), 307, 211, 199. Anal. ($C_{34}H_{36}N_4O \cdot 1/2\ H_2O$) C, H, N.

Molecular Modeling. Molecular modeling calculations were performed on SGI Origin 200 8XR12000, while molecular modeling graphics were carried out on SGI Octane 2 and Octane workstations.

AChE and BuChE crystal structures were downloaded from the PDB data bank (http://www.rcsb.org/pdb/; PDB IDs: 1B41, 1ACJ, 1Q83, 1Q84, 2CEK, 1P0I). Hydrogens were added to all the PDB structures considering a pH value of 7.2. To introduce compounds into both *h*AChE (1B41) and *h*BuChE (1P0I) crystal structures, their ligands, fasciculin-2 and butyrylcholine hydrolysis products, respectively, were removed using the unmerge command in the Biopolymer Module of Insight2005 (Accelrys, San Diego). Water molecules were maintained in the crystal structures with the exception of those that would sterically overlap with the ligand.

The newly designed compounds **3a**−**m** were built using the Insight2005 Builder module. The apparent pK_a values were estimated using the ACD/pK_a DB version 10.00 software (Advanced Chemistry Development Inc., Toronto, Canada). Tacrine moieties of all selected compounds and amine groups of **3b** and **3d**−**h** were considered protonated in all subsequent calculations according to the pK_a values reported in Table 1. Partial charges to protonated compounds were assigned by comparing partial charges assigned by CVFF force field[63] with those estimated by MNDO[64] semiempirical 1 SCF calculations for neutral and the ionized compounds. In particular, CVFF force field partial charges were added to the algebraic difference between MNDO partial charges of the protonated and the neutral forms.

The conformational space of compounds **3a**−**m** was sampled through 200 cycles of simulated annealing (CVFF force field) by following our standard protocol.[37] An initial temperature of 1000 K was applied to the system for 1000 fs with the aim of surmounting torsional barriers; successively temperature was linearly reduced to 200 K with a decrement of 0.5 K/fs. The resulting structures were subjected to energy minimization within Insight2005 Discover module (CVFF force field, conjugate gradient algorithm;[65] ε = 80**r*) until the maximum rms derivative was less than 0.001 kcal/Å and subsequently ranked by their conformational energy values. In particular, the extended conformations with ΔE from the global minimum (ΔE_{GB}) within 20 kcal/mol were taken as ligand starting structures for successive docking.

Refinement of Docking Parameters. Docking parameters were appropriately tailored to the system on the basis of a series of test docking calculations performed on 2CEK, 1ACJ, 1Q83, and 1Q84 AChE crystal structures. In particular, starting from manually modified initial structures, the parameters that were able to reproduce the binding modes of *anti*1 and *syn*1 TZ2PA6 compounds (1Q84 and 1Q83, respectively), compound **2a** (2CEK) and tacrine (1ACJ) to AChE observed in the X-ray crystal structure were chosen. Moreover, different docking procedures were also explored with the aim of investigating if our compounds could induce the same PAS movement observed in the X-ray crystal structures of compound **2a** with *Tc*AChE or compound *syn*1 TZ2PA6 with *m*AChE (2CEK and 1Q83, respectively). In general, the tested parameters considered both the calculation procedure and the complex starting structure. In particular, the following calculation parameters were tested: (i) the energy check method (Metropolis or Energy), and (ii) the nonbond calculation method (cell_multipole, group_based or quartic_vdw_no_coul), (iii) H-bond and van der Waals (vdW) scaling factors, and (iv) the solvation grid. We also modified the complex starting structure by: (i) modifying the protein conformation, (ii) modifying the ligand conformation, and (iii) modifying the size of the *binding domain area* allowed to move during calculations. We used the crystal structure of *h*AChE (PDB: 1B41) as the starting structure and tested different W286 side chain rotamers (Manual_Rotamer command in the Biopolymer module of Insight2005). Final results were ranked by considering: (i) the ΔE value of the putative bioactive conformation of the ligand from its global and relative minimum conformers, and the corresponding rms value (heavy atom superimposition), (ii) final complex binding energy [$E_{binding} = E_{complex} - (E_{protein} + E_{ligand})$], and (iii) the nonbond interaction energies between the ligand and the enzyme (vdW and electrostatic energy contribution; no CUT_OFF option; Discover_3 Module of Insight2005).

Docking Procedure. Docking studies were carried out on compounds **3a**−**m** using a previously applied[37] docking methodology (Affinity, SA_Docking; Insight2005, Accelrys, San Diego) which considers all the systems (i.e., ligand, protein, and water molecules) flexible. Although in the subsequent dynamic docking protocol all the systems were perturbed by means of Monte Carlo and simulated annealing procedures, nevertheless the dynamic docking procedure formally requires a reasonable starting structure. Accordingly, ligands were oriented in the active-site of the enzymes on the basis of previously reported results[37] and for the AChE complexes on the basis of the orientation of tacrine and of compound **2a** in the active-site gorge of *Tc*AChE (PDB code: 1ACJ and 2CEK, respectively).

To obtain more representative results, we further increased the variance of the starting structures used for docking. In particular, since there is an asymmetric distance between the linkers connecting the central functional groups to tacrine moieties in compounds **3c**−**g**, each of these compounds was manually positioned into the active-site gorge of *h*AChE and *h*BuChE either with the **3** or with the **4** methylene linker at the bottom of the gorge, and both resulting structures were used for the following docking procedures.

An energy minimization was performed on each ligand within the active-site using a template force of 10 kcal/Å^2 (conjugate gradient, ϵ = 80**r*, CVFF) and its conformational energy was re-evaluated to ensure that the ΔE_{GB} remained within 20 kcal/mol. A subsequent visual inspection of the resulting low energy conformers, placed in the active-sites of 1B41 and 1P0I, led to the selection of each starting protein−ligand complex. All subsequent structural calculations were performed using the CVFF force field using the previously described ligand partial charge assignment. The obtained complexes were subjected to preliminary energy minimization (steepest descent algorithm; ϵ = 1) until the maximum rms derivative was less than 0.5 kcal/Å to generate roughly docked starting structures, as required by the Affinity docking procedure.

Subsequently, dynamic docking was achieved through the Affinity module in the Insight2005 suite, using the SA_Docking procedure[66] and the Cell_Multipole[67] method for nonbond interactions. A *binding domain area* was defined as a flexible subset around the ligand that was constituted by all residues and water molecules having at least one atom within a 5 Å radius from any given ligand atom. This binding area was enlarged in order to allow the conformational change at the PAS. In particular, in *h*AChE structure, water molecules and residues having at least one atom within 4 Å radius from W286 were added to the binding area. A similar binding domain area of 5 Å around the ligand and 4 Å around F278, was also defined for the BuChE complexes. All atoms included in the *binding domain area* were left free to move during the entire docking calculations. A restrain buffer region is introduced to separate the freely movable atoms and nonmovable atoms: if the closest distance of a movable atom to bulk atoms is less than the sum of their

van der Waals radii plus the 0.5 Å, that movable atom is restrained to its original position using a harmonic restrain force of 100 kcal mol^{-1} $Å^{-1}$.

A Monte Carlo/minimization approach for the random generation of a maximum of 20 acceptable ligand/enzyme complexes, for each compound, was used. During the first step, starting from the previously obtained roughly docked structures (see above), the ligand was moved by a random combination of translation, rotation, and torsional changes (Flexible_Ligand option, considering all rotatable bonds) to sample both the conformational space of the ligand and its orientation with respect to the enzyme (MxRChange = 3 Å; MxAngChange = 180°). During this step, vdW and Coulombic terms were scaled to a factor of 0.1 to avoid very severe divergences in the Coulombic and vdW energies. If the energy of a complex structure resulting from random moves of the ligand was higher by the energy tolerance parameter than the energy of the last accepted structure, it was not accepted for minimization. To ensure a wide variance of the input structures to be successively minimized, an energy tolerance value of 10^6 kcal/mol from the previous structure has been used. After the energy minimization step (conjugate gradient; 2500 iterations; $\varepsilon = 1$), the Metropolis test, at a temperature of 310 K, and a structure similarity check (rms tolerance = 0.3 kcal/Å), were applied to select the 20 acceptable structures. Each subsequent structure was generated from the last accepted structure.

All the accepted complexes resulting from the Monte Carlo/minimization approach were subjected to a molecular dynamics simulated annealing protocol, including 5 ps (ps) of a dynamic run divided in 50 stages (100 fs each) during which the temperature of the system was linearly decreased from 500 to 300 K (Verlet velocity integrator; time step = 1.0 fs). In simulated annealing, the temperature is altered in time increments from an initial temperature to a final temperature. The temperature is changed by adjusting the kinetic energy of the structure (by rescaling the velocities of the atoms). Molecular dynamics calculations were performed using a constant temperature and constant volume (*NVT*) statistical ensemble, and the direct velocity scaling as temperature control method (Temp Window = 10 K). In the first stage, initial velocities were randomly generated from Boltzmann distribution, according to the desired temperature, while during the subsequent stages initial velocities were generated from Dynamics Restart Data. The temperature of 500 K was applied with the aim of surmounting torsional barriers, thus allowing an unconstrained rearrangement of the ligand and the protein active site (initial vdW and Coulombic scale factors = 0.1). Successively temperature was linearly reduced to 300 K in 5 ps, and concurrently the scale factors have been similarly decreased from their initial values (0.1) to their final values (1.0). A final round of 10^5 minimization steps (conjugate gradient, $\epsilon = 1$) followed the last dynamics steps, and the minimized structures were saved in a trajectory file. The ligand/enzyme complexes thus obtained were ranked by considering: (i) the ΔE value of the resulting bioactive conformation of the ligand, from its global and relative minimum conformers, and the corresponding rms value (heavy atom superimposition), (ii) final complex binding energy [$E_{binding} = E_{complex} - (E_{protein} + E_{ligand})$], and (iii) the nonbond interaction energies between the ligand and the enzyme (vdW and electrostatic energy contribution; no CUT_OFF option; Discover_3 Module of Insight2005).

To finally select the complex representing the most probable enzyme−ligand binding mode, after the docking procedure, the lowest energy complexes presenting higher enzyme−ligand interaction energies were further minimized (CVFF forcefield, $\epsilon = 1$) by a combination of Steepest Descent (maximum rms derivative less than 0.1 kcal/Å) and conjugate gradient algorithms (maximum rms derivative less than 0.01 kcal/Å) to allow the relaxation of the whole protein, and resubjected to the above-reported structural and energy evaluation. The geometry of $\pi-\pi$ interactions was evaluated considering:[68−71] (i) the distance between the centroids of the aromatic rings, (ii) the angle between the planes of the rings, (iii) the offset value, and (iv) the direction of the dipole vectors.

Bioinformatics Analysis. All *Tc*AChE, *m*AChE, and *h*AChE crystal structures were downloaded from the PDB data bank (http://www.rcsb.org/pdb/). Hydrogens were added to all the PDB structures considering a pH value of 7.2. A summary of the crystal structures analyzed is reported in Table 1 of the Supporting Information.

To compare the flexibility of several residues observed in our docking studies with those observed in the AChE crystal structures, the dihedral angles of the backbone (φ and ψ) and side chains ($\chi1$ and $\chi2$) for these residues were calculated and tabulated using the Residue_Dihedral command (Homology Module, Insight2005). In particular, the following residues were considered for AChE: Y72, D74, W86, G120-G122, Y124, W286, Y337, Y341, and Y449 (*h*AChE numbering). The calculated dihedral angle values for the considered crystal structures and our docked complexes, are reported in Table 2 of the Supporting Information. The X-ray crystal structures of *Torpedo californica*, mouse, and human AChE were grouped depending on the absence or presence of an inhibitor, and in the latter case on the type of inhibitor. Subsequently, all structures, (including our docked complexes) were grouped into families on the basis of the calculated dihedral angle for a residue using: (i) reference values from the structures of the native forms of *Tc*AChE and *m*AChE (PDB code: 1EA5 and 1J06, respectively), and (ii) an increment (Δ value) of 30° from the reference value.

The linear functional motifs present in *h*AChE and *h*BuChE were identified using the Eukaryotic Linear Motif server http://elm.eu.org/, a resource for predicting small functional sites in eukaryotic proteins such as those subject to post-translational modifications or involved in protein−protein interactions.[72]

The experimentally determined structure of SH3 domains (PDB IDs: 1QWE, 1QWF) and LxxLL motifs (PDB IDs: 1SB0, 1T7F) were downloaded from the Protein Data Bank (PDB; http://www.rcsb.org/pdb/) and analyzed by the ConSeq Server (http://conseq.bioinfo.tau.ac.il). The Cα and side chain centroid distances between the interacting residues were calculated as reference values for the subsequent analysis of the *h*AChE and *h*BuChE structures. The identification of SH3-like interaction residues in *h*AChE and *h*BuChE and the calculation of their Cα and centroid distances were performed by using an "home made" command file (Insight2005, Accelrys, San Diego).

Quantitation of Anticholinesterase Activity. The inhibitory activity of the new tacrine-related compounds was evaluated using purified recombinant *h*AChE and *h*BuChE. AChE and BuChE activities were measured in 50 mM sodium phosphate, pH 8.0, at 25 °C as described using acetylthiocholine and butyrylthiocholine as substrates, respectively.[73] Inhibition of enzyme activity was measured over a substrate concentration range of 0.01−30 mM and at least six inhibitor concentrations. Plots of initial velocities versus substrate concentrations at a series of inhibitor concentrations were analyzed by nonlinear least-squares methods to determine the values of K_m (Michaelis−Menten constant) and V_{max} (maximal velocity). Nonlinear regression analysis of the plots of V_{max}/K_m values versus [Inhibitor] were used for the determination of K_i values.[73]

Acknowledgment. The authors thank the European Research Centre for Drug Discovery and Development and MIUR Prin for financial support. The opinions or assertions contained herein are the private views of the authors and are not to be construed as official or as reflecting true views of the Department of the Army or the Department of Defense.

Supporting Information Available: The 87 analyzed AChE X-ray crystal structures available in the PDB, results of bioinformatics analysis, binding energies, figures of additional docking results, and elemental analyses for title compounds, are available free of charge via the Internet at http://pubs.acs.org.

References

(1) Hebert, L. E.; Scherr, P. A.; Bienias, J. L.; Bennett, D. A.; Evans, D. A. Alzheimer disease in the U.S. population: prevalence estimates using the 2000 census. *Arch. Neurol.* **2003**, *60*, 1119–1122.

(2) Rocchi, A.; Pellegrini, S.; Siciliano, G.; Murri, L. Causative and susceptibility genes for Alzheimer's disease: a review. *Brain Res. Bull.* **2003**, *61*, 1–24.

(3) Bowen, D. M.; Allen, S. J.; Benton, J. S.; Goodhardt, M. J.; Haan, E. A.; Palmer, A. M.; Sims, N. R.; Smith, C. C.; Spillane, J. A.; Esiri, M. M.; Neary, D.; Snowdon, J. S.; Wilcock, G. K.; Davison, A. N. Biochemical assessment of serotonergic and cholinergic dysfunction and cerebral atrophy in Alzheimer's disease. *J. Neurochem.* **1983**, *41*, 266–272.

(4) Giacobini, E. Cholinesterase inhibitors: new roles and therapeutic alternatives. *Pharmacol. Res.* **2004**, *50*, 433–440.

(5) Tasker, A.; Perry, E. K.; Ballard, C. G. Butyrylcholinesterase: impact on symptoms and progression of cognitive impairment. *Expert Rev. Neurother.* **2005**, *5*, 101–106.

(6) Giacobini, E. Cholinergic functions in Alzheimer's disease. *Int. J. Geriatr. Psychiatry* **2003**, *18*, S1−S5 and references therein.

(7) Lane, R. M.; Potkin, S. G.; Enz, A. Targeting acetylcholinesterase and butyrylcholinesterase in dementia. *Int. J. Neuropsychopharmacol.* **2006**, *1*, 101–124.

(8) (a) Greig, N. H.; Utsuki, T.; Ingram, D. K.; Wang, Y.; Pepeu, G.; Scali, C.; Yu, Q. S.; Mamczarz, J.; Holloway, H. W.; Giordano, T.; Chen, D.; Furukawa, K.; Sambamurti, K.; Brossi, A.; Lahiri, D. K. Selective butyrylcholinesterase inhibition elevates brain acetylcholine, augments learning and lowers Alzheimer-amyloid peptide in rodent. *Proc. Natl. Acad. Sci. U.S.A.* **2005**, *102*, 17213–17218. (b) Bartorelli, L.; Giraldi, C.; Saccardo, M.; Cammarata, S.; Bottini, G.; Fasanaro, A. M.; Trequattrini, A. Effects of switching from an AChE inhibitor to a dual AChE-BuChE inhibitor in patients with Alzheimer's disease. *Curr. Med. Res. Opin.* **2005**, *21*, 1809–1818. (c) Grossberg, G. Effect of rivastigmine in the treatment of behavioral disturbances associated with dementia: review of neuropsychiatric impairment in Alzheimer's disease. *Curr. Med. Res. Opin.* **2005**, *21*, 1631–1639.

(9) (a) Mesulam, M. M.; Guillozet, A.; Shaw, P.; Levey, A.; Duysen, E. G.; Lockridge, O. Acetylcholinesterases knockouts establish central cholinergic pathways and can use butyrylcholinesterase to hydrolyze acetylcholine. *Neuroscience* **2002**, *110*, 627–639. (b) Xie, W.; Stribley, J. A.; Chatonnet, A.; Wilder, P. J.; Rizzino, A.; McComb, R. D.; Taylor, P.; Hinrichs, S. H.; Lockridge, O. Postnatal developmental delay and supersensitivity to organophosphate in gene-targeted mice lacking acetylcholinesterase. *J. Pharmacol. Exp. Ther.* **2000**, *293*, 896–902. (c) Li, B.; Stribley, J. A.; Ticu, A.; Xie, W.; Schopfer, L. M.; Hammond, P.; Brimijoin, S.; Hinrichs, S. H.; Lockridge, O. Abundant tissue butyrylcholinesterase and its possible function in the acetylcholinesterase knockout mouse. *J. Neurochem.* **2000**, *75*, 1320–1331. (d) Giacobini, E.; Cholinesterase inhibitors: from the Calabar bean to Alzheimer therapy. In: *Cholinesterases and Cholinesterase Inhibitors*; Giacobini, E., Ed.; Martin Duniz Ltd.: London, 2000, Vol. 18, pp 1−226.

(10) Ballard, C. G.; Perry, E. K. The role of butyrylcholinesterase in Alzheimer's disease. In *Butyrylcholinesterase: Its Function and Inhibitors*; Giacobini, E., Ed.; Martin Dunitz Ltd.: London 2003; Vol. 123, p 134.

(11) Ballard, C. G. Advances in the treatment of Alzheimer's disease: benefits of dual cholinesterase inhibition. *Eur. Neurol.* **2002**, *47*, 64–70.

(12) Legay, C.; Huchet, M.; Massoulié, J.; Changeux, J. P. Developmental regulation of acetylcholinesterase transcripts in the mouse diaphragm: alternative splicing and focalization. *Eur. J. Neurosci* **1995**, *7*, 1803–1809.

(13) Perrier, A. L.; Massoulie, J.; Krejci, E. PRiMA: The membrane anchor of acetylcholinesterase in the brain. *Neuron* **2002**, *33*, 275–285.

(14) Inestrosa, N. C.; Sagal, J. P.; Colombres, M. Acetylcholinesterase interaction with Alzheimer amyloid beta. *Subcell Biochem.* **2005**, *38*, 299–317.

(15) Meshorer, E.; Soreq, H. Virtues and woes of AChE alternative splicing in stress-related neuropathologies. *Trends Neurosci.* **2006**, *29*, 216–224.

(16) Blong, R. M.; Bedows, E.; Lockridge, O. Tetramerization domain of human butyrylcholinesterase is at the C-terminus. *Biochem. J.* **1997**, *327*, 747–757.

(17) Silman, I.; Sussman, J. L. Acetylcholinesterase: "classical" and "nonclassical" functions and pharmacology. *Curr. Opin. Pharmacol.* **2005**, *5*, 293–302.

(18) (a) Soreq, H.; Seidman, S. Acetylcholinesterase: new roles for an old actor. *Nature* **2001**, *2*, 294–302. (b) Small, D. H.; Reed, G.; Whitfield, B.; Nurcombe, V. Cholinergic regulation of neurite outgrowth from isolated chick sympathetic neurones in culture. *J. Neurosci.* **1995**, *15*, 144–151.

(19) Wilson, D. B. The effects of zinc on the multicatalytic activities of acetylcholinesterase and butyrylcholinesterase. Thesis presented to the Faculty of Graduate Studies, University of Guelph, Guelph, Ontario, Canada, 1997.

(20) Tsigelny, I.; Shindyalov, I. N.; Bourne, P. E.; Sudhof, T. C.; Taylor, P. Common EF-hand motifs in cholinesterases and neuroligins suggest a role for Ca^{2+} binding in cell surface associations. *Protein Sci.* **2000**, *9*, 180–185.

(21) Inestrosa, N. C.; Alvarez, A.; Perez, C. A.; Moreno, R. D.; Vicente, M.; Linker, C.; Casanueva, O. I.; Soto, C.; Garrido, J. Acetylcholinesterase accelerates assembly of amyloid-beta-peptides into Alzheimer's fibrils: possible role of the peripheral site of the enzyme. *Neuron* **1996**, *16*, 881–891.

(22) Reyes, A. E.; Perez, D. R.; Alvarez, A.; Garrido, J.; Gentry, M. K.; Doctor, B. P.; Inestrosa, N. C. A monoclonal antibody against acetylcholinesterase inhibits the formation of amyloid fibrils induced by the enzyme. *Biochem. Biophys. Res. Commun.* **1997**, *232*, 652–655.

(23) Bartolini, M.; Bertucci, C.; Cavrini, V.; Andrisano, V. Beta-amyloid aggregation induced by human acetylcholinesterase: inhibition studies. *Biochem. Pharmacol.* **2003**, *65*, 407–416.

(24) Reyes, A. E.; Chacon, M. A.; Dinamarca, M. C.; Cerpa, W.; Morgan, C.; Inestrosa, N. C. Acetylcholinesterase−Ab complexes are more toxic than Ab fibrils in rat hippocampus: effect on rat beta-amyloid aggregation, laminin expression, reactive astrocytosis, and neuronal cell loss. *Am. J. Pathol.* **2004**, *164*, 2163–2174.

(25) Bui, J. M.; Tai, K.; McCammon, J. A. Acetylcholinesterase: enhanced fluctuations and alternative routes to the active site in the complex with fasciculin-2. *J. Am. Chem. Soc.* **2004**, *126*, 7198–7205.

(26) (a) Shi, J.; Boyd, A. E.; Radic, Z.; Taylor, P. Reversibly bound and covalently attached ligands induce conformational changes in the omega loop, Cys69−Cys96, of mouse acetylcholinesterase. *J. Biol. Chem.* **2001**, *276*, 42196–42204. (b) Bourne, Y.; Radic, Z.; Sulzenbacher, G.; Kim, E.; Taylor, P.; Marchot, P. Substrate and product trafficking through the active center gorge of acetylcholinesterase analyzed by crystallography and equilibrium binding. *J. Biol. Chem.* **2006**, *281*, 29256–29267.

(27) (a) Weiner, L.; Kreimer, D.; Roth, E.; Silman, I. Oxidative stress transfoms acetylcholinesterase to a molten-globule-like state. *Biochem. Biophys. Res. Commun.* **1994**, *198*, 915–922. (b) Millard, C. B.; Shnyrov, V. L.; Newstead, S.; Shin, I.; Roth, E.; Silman, I.; Weiner, L. Stabilization of a metastable state of *Torpedo californica* acetylcholinesterase by chemical chaperones. *Protein Sci.* **2003**, *12*, 2337–2347.

(28) (a) Shi, J.; Tai, K.; McCammon, J. A.; Taylor, P.; Johnson, D. A. Nanosecond dynamics of the mouse acetylcholinesterase Cys69−Cys96 omega loop. *J. Biol. Chem.* **2003**, *278*, 30905–30911. (b) Kua, J.; Zhang, Y.; McCammon, J. A. Studying enzyme binding specificity in acetylcholinesterase using a combined molecular dynamics and multiple docking approach. *J. Am. Chem. Soc.* **2002**, *124*, 8260–8267. (c) Senapati, S.; Bui, J. M.; McCammon, J. A. Induced fit in mouse acetylcholinesterase upon binding a femtomolar inhibitor: a molecular dynamics study. *J. Med. Chem.* **2005**, *48*, 8155–6812. (d) Zhou, H. X.; Wlodek, S. T.; McCammon, J. A. Conformation gating as a mechanism for enzyme specificity. *Proc. Natl. Acad. Sci. U.S.A.* **1998**, *95*, 9280–9283. (e) Tai, K.; Shen, T.; Henchman, R. H.; Bourne, Y.; Marchot, P.; McCammon, J. A. Mechanism of acetylcholinesterase inhibition by fasciculin: a 5 ns molecular dynamics simulation. *J. Am. Chem. Soc.* **2002**, *124*, 6153–6161. (g) Gilson, M. K.; Straatsma, T. P.; McCammon, J. A.; Ripoll, D. R.; Faerman, C. H.; Axelsen, P. H.; Silman, I.; Sussman, J. L. Open "back door" in a molecular dynamics simulation of acetylcholinesterase. *Science* **1994**, *263*, 1276–1278. (h) Wlodek, S. T.; Clark, T. W.; Scott, L. R.; McCammon, J. A. Molecular dynamics of acetylcholinesterase dimer complexed with tacrine. *J. Am. Chem. Soc.* **1997**, *119*, 9513–9522. (i) Shen, T.; Tai, K.; Henchman, R. H.; McCammon, J. A. Molecular dynamics of acetylcholinesterase. *Acc. Chem. Res.* **2002**, *35*, 332–340. (j) Senapati, S.; Cheng, Y.; McCammon, J. A. In situ synthesis of a tacrine-triazole-based inhibitor of acetylcholinesterase: configurational selection imposed by steric interactions. *J. Med. Chem.* **2006**, *49*, 6222–6230.

(29) Shi, J.; Radic, Z.; Taylor, P. Inhibitors of different structure induce distinguishing conformations in the omega loop, Cys69−Cys96, of mouse acetylcholinesterase. *J. Biol. Chem.* **2002**, *277*, 43301–43308.

(30) Radic, Z.; Quinn, D. M.; Vellom, D. C.; Camp, S.; Taylor, P. Allosteric control of acetylcholinesterase catalysis by fasciculin. *J. Biol. Chem.* **1995**, *270*, 20391–20399.

(31) Bourne, Y.; Radic, Z.; Kolb, H. C.; Sharpless, K. B.; Taylor, P.; Marchot, P. Structural insights into conformational flexibility at the peripheral site and within the active center gorge of AChE. *Chem. Biol. Interact.* **2005**, *15*, 159–165.

(32) Barak, D.; Ordentlich, A.; Bromberg, A.; Kronman, C.; Marcus, D.; Lazar, A.; Ariel, N.; Velan, B.; Shafferman, A. Allosteric modulation of acetylcholinesterase activity by peripheral ligands involves a

conformational transition of the anionic subsite. *Biochemistry* **1995**, *34*, 15444–15452.
(33) Velan, B.; Barak, D.; Ariel, N.; Leitner, M.; Bino, T.; Ordentlich, A.; Shafferman, A. Structural modifications of the omega loop in human acetylcholinesterase. *FEBS Lett.* **1996**, *395*, 22–28.
(34) Shi, J.; Boyd, A. E.; Radic, Z.; Taylor, P. Reversibly bound and covalently attached ligands induce conformational changes in the omega loop, Cys69−Cys96, of mouse acetylcholinesterase. *J. Biol. Chem.* **2001**, *276*, 42196–42204.
(35) Arkin, M. R.; Wells, J. A. Small-molecule inhibitors of protein−protein interactions: progressing towards the dream. *Nat. Rev. Drug Discovery* **2004**, *3*, 301–317.
(36) Gonzales-Ruiz, D.; Golhke, H. Targeting protein−protein interactions with small molecules: challenges and perspectives for computational binding epitope detection and ligand finding. *Curr. Med. Chem.* **2006**, *13*, 2607–2625.
(37) (a) Savini, L.; Gaeta, A.; Fattorusso, C.; Catalanotti, B.; Campiani, G.; Chiasserini, L.; Pellerano, C.; Novellino, E.; McKissic, D.; Saxena, A. Specific targeting of acetylcholinesterase and butyrylcholinesterase recognition sites. Rational design of novel, selective, and highly potent cholinesterase inhibitors. *J. Med. Chem.* **2003**, *46*, 1–4. (b) Campiani, G.; Fattorusso, C.; Butini, S.; Gaeta, A.; Agnusdei, M.; Gemma, S.; Persico, M.; Catalanotti, B.; Savini, L.; Nacci, V.; Novellino, E.; Holloway, H. W.; Greig, N. H.; Belinskaya, T.; Fedorko, J. M.; Saxena, A. Development of molecular probes for the identification of extra interaction sites in the mid-gorge and peripheral sites of butyrylcholinesterase (BuChE). Rational design of novel, selective, and highly potent BuChE inhibitors;. *J. Med. Chem.* **2005**, *48*, 1919–1929.
(38) Bourne, Y.; Kolb, H. C.; Radic, Z.; Sharpless, K. B.; Taylor, P.; Marchot, P. Freeze-frame inhibitor captures acetylcholinesterase in a unique conformation. *Proc. Natl. Acad. Sci. U.S.A.* **2004**, *101*, 1449–1454.
(39) Soldi, G.; Plakoutsi, G.; Taddei, N.; Chiti, F. Stabilization of a native protein mediated by ligand binding inhibits amyloid formation independently of the aggregation pathway. *J. Med. Chem.* **2006**, *49*, 6057–6064.
(40) Carlier, P. R.; Du, D. M.; Han, Y.; Liu, J.; Pang, Y. P. Potent, easily synthesized huperzine A-tacrine hybrid acetylcholinesterase inhibitors. *Bioorg. Med. Chem. Lett.* **1999**, *9*, 2335–2338.
(41) Jonckers, T. H. M.; Maes, B. U. W.; Lemière, G. L. F.; Rombotus, G.; Pieters, L.; Haemers, A.; Dommisse, R. A. Synthesis of isocryptolepine via Pd-catalyzed "amination arylation" approach. *Synlett* **2003**, *5*, 615–613.
(42) Finlander, P.; Fischer, H. P.; Pedersen, E. B. Phosphorus pentoxide in organic synthesis part 23: synthesis of 1,2,3,4-tetrahydro-9-acridinamines. *Heterocycles* **1985**, *23*, 1437–1444.
(43) Jakus, J.; Wolff, E. C.; Park, M. H.; Folk, J. E. Features of the spermidine-binding site of deoxyhypusine synthase as derived from inhibition studies. Effective inhibition by bis- and mono-guanylated diamines and polyamines. *J. Biol. Chem.* **1993**, *268*, 13151–13159.
(44) Hay, M. P.; Pruijn, F. B.; Gamage, S. A.; Liyanage, H. D. S.; Kovacs, M. S.; Patterson, A. V.; Wilson, W. R.; Brown, J. M.; Denny, W. A. DNA-targeted 1,2,4-benzotriazine 1,4-dioxides: Potent analogues of the hypoxia-selective cytotoxin tirapazamine. *J. Med. Chem.* **2004**, *47*, 475–488.
(45) Atasoy, B.; Özen, R. Synthesis of 3,4-disubstituted furans via unsaturated cyclic peroxides arising by photooxygenation of 2,3-bis(bromomethyl)-l,3-butadiene and derived exocyclic dienes. *Tetrahedron* **1997**, *53*, 13867–13872.
(46) Campiani, G.; Butini, S.; Trotta, F.; Aiello, F.; Fattorusso, C.; Catalanotti, B.; Nacci, V.; Novellino, E.; Stark, J. A.; Cagnotto, A.; Fumagalli, E.; Carnovali, F.; Cervo, L.; Mennini, T. Synthesis and pharmacological evaluation of potent and highly selective D_3 receptor ligands: inhibition of cocaine-seeking behaviour and the role of dopamine D_3/D_2 receptors. *J. Med. Chem.* **2003**, *46*, 3822–3839.
(47) Jenneskens, L. W.; Kostermans, G. B. M.; ten Brink, H. J.; de Wolf, W. H.; and Bickelhaupt, F. The synthesis of hetero-bridged[5]-(3,6)oxapinophanes. *J. Chem. Soc. Perkin Trans 1* **1985**, 2119–2122.
(48) Caddick, S.; Judd, D. B.; de, K.; Lewis, A. K.; Reich, M. T.; Williams, M. R. V. A generic approach for the catalytic reduction of nitriles. *Tetrahedron* **2003**, *59*, 5417–5423.
(49) Khurana, J. M.; Kukreja, G. Rapid reduction of nitriles to primary amines with nickel boride at ambient temperature. *Synth. Commun.* **2002**, *32*, 1265–1269.
(50) Colletier, J. P.; Sanson, B.; Nachon, F.; Gabellieri, E.; Fattorusso, C.; Campiani, G.; Weik, M. Conformational flexibility in the peripheral site of *Torpedo californica* acetylcholinesterase revealed by the complex structure with a bifunctional inhibitor. *J. Am. Chem. Soc.* **2006**, *128*, 4526–4527.
(51) Rydberg, E. H.; Brumshtein, B.; Greenblatt, H. M.; Wong, D. M.; Shaya, D.; Williams, L. D.; Carlier, P. R.; Pang, Y. P.; Silman, I.; Sussman, J. L. Complexes of alkylene-linked tacrine dimers with *Torpedo californica* acetylcholinesterase: binding of bis(5)-tacrine produces a dramatic rearrangement in the active-site gorge. *J. Med. Chem.* **2006**, *49*, 5491–5500.
(52) Scholl, F. G.; Scheiffele, P. Making connections: cholinesterase-domain proteins in the CNS. *Trends Neurosci.* **2003**, *26*, 618–624.
(53) Berezin, C.; Glaser, F.; Rosenberg, J.; Paz, I.; Pupko, T.; Fariselli, P.; Casadio, R.; Ben-Tal, N. ConSeq: The identification of functionally and structurally important residues in protein sequences. *Bioinformatics* **2004**, *20*, 1322–1324.
(54) Feng, S.; Kasahara, C.; Rickles, R. J.; Schreiber, S. L. Specific interactions outside the proline-rich core of two classes of Src homology 3 ligands. *Proc. Natl. Acad. Sci. U.S.A.* **1995**, *92*, 12408–12415.
(55) Heuer, K.; Kofler, M.; Langdon, G.; Thiemke, K.; Freund, C. Structure of a helically extended SH3 domain of the T cell adapter protein ADAP. *Structure* **2004**, *12*, 603–610.
(56) Mayer, B. J. SH3 domains: complexity in moderation. *J. Cell Sci.* **2001**, *114*, 1253–1263.
(57) Hur, E.; Pfaff, S. J.; Payne, E. S.; Gron, H.; Buehrer, B. M.; Fletterick, R. J. Recognition and accommodation at the androgen receptor coactivator binding interface. *PLoS Biol.* **2004**, *2*, E274.
(58) Dubbink, H. J.; Hersmus, R.; Verma, C. S.; Van der Korput, H. A.; Berrevoets, C. A.; Van Tol, J.; Ziel-van der Made, A. C.; Brinkmann, A. O.; Pike, A. C.; Trapman, J. Distinct recognition modes of FXXLF and LXXLL motifs by the androgen receptor. *Mol. Endocrinol.* **2004**, *18*, 2132–2150.
(59) Greiner, E. F.; Kirfel, J.; Greschik, H.; Huang, D.; Becker, P.; Kapfhammer, J. P.; Schule, R. Differential ligand-dependent protein−protein interactions between nuclear receptors and a neuronal-specific cofactor. *Proc. Natl. Acad. Sci. U.S.A.* **2000**, *97*, 7160–7165.
(60) He, B.; Kemppainen, J. A.; Wilson, E. M. FXXLF and WXXLF sequences mediate the NH_2-terminal interaction with the ligand binding domain of the androgen receptor. *J. Biol. Chem.* **2000**, *275*, 22986–22994.
(61) Sol, V.; Lamarche, F.; Enache, M.; Garcia, G.; Granet, R.; Guilloton, M.; Blais, J. C.; Krausz, P. Polyamine conjugates of *meso*-tritolylporphyrin and protoporphyrin IX: potential agents for photodynamic therapy of cancers. *Bioorg. Med. Chem.* **2006**, *14*, 1364–1377.
(62) Chen, D.; Martel, A. E.; McManus, D. Studies of the mechanism of chelate degradation in iron-based, liquid redox H_2S removal processes. *Can. J. Chem.* **1995**, *73*, 264–274.
(63) Dauber-Osguthorpe, P.; Roberts, V. A.; Osguthorpe, D. J.; Wolff, J.; Genest, M.; Hagler, A. T. Structure and energetics of ligand binding to proteins: *E. coli* dihydrofolate reductase-trimethoprim, a drug-receptor system. *Proteins* **1988**, *4*, 31–47.
(64) Dewar, M. J. S.; Thiel, W. Ground states of molecules. 38. The MNDO method. Approximations and parameters. *J. Am. Chem. Soc.* **1977**, *99*, 4899–4907.
(65) Fletcher, R. Unconstrained Optimization. In *Practical Methods of Optimization*; John Wiley & Sons: New York 1980; Vol. 1.
(66) Senderowitz, H.; Guarnieri, F.; Still, W. C. A smart Monte Carlo technique for free energy simulations of multiconformational molecules. Direct calculations of the conformational populations of organic molecules. *J. Am. Chem. Soc.* **1995**, *117*, 8211–8219.
(67) Ding, H. Q.; Karasawa, N.; Goddard, W. A III Atomic level simulations on a million particles: the cell multipole method for Coulomb and London non-bond interactions. *J. Chem. Phys.* **1992**, *97*, 4309–4315.
(68) Singh, J.; Thornton, J. M. SIRIUS. An automated method for the analysis of the preferred packing arrangements between protein groups. *J. Mol. Biol.* **1990**, *211*, 595–615.
(69) Hunter, C. A.; Lawson, K. R.; Perkins, J.; Urch, C. J. Aromatic interactions. *J. Chem. Soc., Perkin Trans. 1* **2001**, *2*, 651–669.
(70) Cubero, E.; Luque, J. F.; Orozco, M. Is polarization important in cation-p interactions. *Proc. Natl. Acad. Sci. U.S.A.* **1998**, *95*, 5976–5980.
(71) Kim, K. S.; Tarakeshwar, P.; Yong Lee, J. Molecular clusters of p-systems: theoretical studies of structures, spectra, and origin of interaction energies. *Chem. Rev.* **2000**, *100*, 4145–4185.
(72) Puntervoll, P.; Linding, R.; Gemund, C.; Chabanis-Davidson, S.; Mattingsdal, M.; Cameron, S.; Martin, D. M.; Ausiello, G.; Brannetti, B.; Costantini, A.; Ferre, F.; Maselli, V.; Via, A.; Cesarei, G.; Diella, F.; Superti-Furga, G.; Wyrwicz, L.; Ramu, C.; McGuigan, C.; Gudavalli, R.; Letunic, I.; Bork, P.; Rychlewski, L.; Kuster, B.; Helmer-Citterich, M.; Hunter, W. N.; Aasland, R.; Gibson, T. J. ELM server: A new resource for investigating short functional sites in modular eukaryotic proteins. *Nucleic Acids Res.* **2003**, *31*, 3625–3630.
(73) Gemma, S.; Gabellieri, E.; Huleatt, P. B.; Fattorusso, C.; Borriello, M.; Catalanotti, B.; Butini, S.; De Angelis, M.; Novellino, E.; Nacci, V.; Belinskaya, T.; Saxena, A.; Campiani, G. Discovery of huperzine A/tacrine hybrids as potent inhibitors of human cholinesterases targeting their mid-gorge recognition sites. *J. Med. Chem.* **2006**, *49*, 3421–3425.

JM701253T